ČESKÉ VYSOKÉ UČENÍ TECHNICKÉ V PRAZE

FAKULTA JADERNÁ A FYZIKÁLNĚ INŽENÝRSKÁ

K A T E D R A M A T E R I Á L Ů

MORPHOLOGICAL AND STRUCTURAL CHANGES OF CERAMIC POWDERS DURING PLASMA SPRAYING

DIPLOMOVÁ PRÁCE

Autor :

Bc. Jonáš DUDÍK

Vedoucí práce :

Ing. Radek MUŠÁLEK, Ph.D.

Vedoucí katedry :

doc. Ing. Aleš MATERNA, Ph.D.

Stran : 67

Obrázků : 35

Tabulek : 11

Praha, 7. července 2022

Číslo kopie :

České vysoké učení technické v Praze, Fakulta jaderná a fyzikálně inženýrská

Katedra: materiálů Akademický rok: 2021/2022

ZADÁNÍ DIPLOMOVÉ PRÁCE

Student: Bc. Jonáš Dudík

Studijní program : Fyzikální inženýrství materiálů

Specializace:

Název práce: (česky) Morfologické a strukturní změny keramických prášků během plazmového stříkání

Název práce: (anglicky) Morphological and Structural Changes of Ceramic Powders during Plasma Spraying

Pokyny pro vypracování:

1) Vypracujte rešerši o metodikách používaných při studiu morfologie, chemického složení a struktury práškových materiálů s přihlédnutím k metodám dostupným na ÚFP AV ČR a KMAT-FJFI-ČVUT v Praze.
2) Navrhněte metodiku a konstrukční řešení pro záchyt materiálů po průchodu plazmatem.
3) Navrženou metodiku ověřte pro vybrané keramiky podávané ve formě prášku, suspenze, roztoku, resp. jejich kombinací (hybridní plazmové stříkání).
4) Proveďte charakterizaci získaných vzorků a srovnejte je s výchozími materiály.
5) Diskutujte vliv procesních parametrů na vlastnosti výsledných prášků.
6) Získané výsledky porovnejte s literaturou a přehledně zpracujte.
7) Zhodnoťte vhodnost navržené metodiky pro její případné průmyslové použití, např. přípravu nových materiálů, atomizaci, apod.

Doporučená literatura:

[1] J.R. Davis, Handbook of Thermal Spray Technology, ASM International, 2004
[2] L. Pawlowski, The Science and Engineering of Thermal Spray Coatings, John Wiley & Sons, 1995
[3] J. Kotlan, Z. Pala, R. Musalek, P. Ctibor, On Reactive Suspension Plasma Spraying of Calcium Titanate, Ceram. Int., 2016, 42 (3), p 4607–4615
[4] K. Volenik, F. Hanousek, P. Chraska, J. Ilavsky, K. Neufuss, In-Flight Oxidation of High-Alloy Steels during Plasma Spraying, Mater. Sci. Eng. A, 1999, 272 (1), p 199–206
[5] J. Medricky, R. Musalek, M. Janata, T. Chraska, and F. Lukac, Cost-Effective Plasma Spraying for Large-Scale Applications, in ITSC 2018 - Proc. Int. Therm. Spray Conf., 2018, p 683–689
[6] S. Kumar, V. Selvarajan, P.V.A. Padmanabhan, K.P. Sreekumar, Spheroidization of Metal and Ceramic Powders in Thermal Plasma Jet: Comparison between Experimental Results and Theoretical Estimation, J. Mater. Process. Technol., 2006, 176 (1–3), p 87–94
[7] Y. Li, K.A. Khor, Effect of Plasma Spraying Conditions on the Spheroidization of Zircon and Alumina Mixtures, J. Mater. Process. Technol., 1999, 89–90 p 532–537
[8] X. Zhang, K. Zhou, F. Chang, C. Song, C. Deng, S. Liang, Yttria-Stabilized-Zirconia Hollow Spheres Prepared by Atmospheric Plasma Spray, Particuology, 2014, 14 p 57–62

Jméno a pracoviště vedoucího práce:

Ing. Radek Mušálek, Ph.D., Ústav fyziky plazmatu AV ČR, v.v.i. Oddělení materiálového inženýrství

Jméno a pracoviště konzultanta:

Ing. Jan Medřický, Ph.D., Ústav fyziky plazmatu AV ČR, v.v.i.
Ing. Tomáš Tesař, Ústav fyziky plazmatu AV ČR, v.v.i.

Datum zadání diplomové práce: 30. 9. 2021

Termín odevzdání diplomové práce: 2. 5. 2022

Doba platnosti zadání je dva roky od data zadání

V Praze dne 30. 9. 2021

garant studijního programu

vedoucí katedry

děkan

Prohlášení.

Prohlašuji, že jsem svou diplomovou práci vypracoval samostatně a použil jsem pouze podklady (literaturu, projekty, software, atd.) uvedené v přiloženém seznamu.

Nemám závažný důvod proti užití tohoto školního díla ve smyslu §60 Zákona č.121/2000 Sb. (a jeho novel č. 81/2005 Sb. a 216/2006 Sb.) o právu autorském.

V Praze dne 7. 7. 2022 Podpis:

Poděkování

Na tomto místě bych rád poděkoval Ing. Radku Mušálkovi, Ph.D. za vlídný a velmi trpělivý přístup. Neméně trpělivý byl i Ing. Tomáš Tesař, Ph.D. při předávání četných rad a vědomostí, stejně jako při korektuře textu. Tomášovi a Ing. Janu Medřickému, Ph.D. děkuji také za doprovod při provádění veškerých experimentů a Honzovi především za vedení při výrobě experimentálního zařízení pro tuto práci.

Dále bych rád poděkoval Romainu Génois, Ph.D. a RNDr. Františkovi Lukáčovi, Ph.D. za provedená XRD a XRF měření a konzultace k těmto metodám. Děkuji také kolektivu v LPT za zajištění provozu samotných experimentů. Důležití při tvorbě této práce byli také ostatní členové kolektivu na IPP, kteří vždy tvořili přátelské prostředí a nabízeli pomocné ruce.

Na závěr patří poděkování samozřejmě mé rodině a přítelkyni za dlouhodobou podporu, díky kterým jsem se vždy mohl věnovat studiu naplno. Při studiu mě pak provázelo několik přátel – spolužáků, díky kterým jsem se dostal až k dokončení této práce.

Název práce:
Morfologické a strukturní změny keramických prášků během plazmového stříkání

Autor: Bc. Jonáš Dudík

Obor: Fyzikální inženýrství
Druh práce: Diplomová práce

Vedoucí práce: Ing. Radek Mušálek, Ph.D. Oddělení materiálového inženýrství, Ústav fyziky plazmatu AV ČR, v.v.i.

Konzultant: Ing. Tomáš Tesař, Ph.D. Oddělení materiálového inženýrství, Ústav fyziky plazmatu AV ČR, v.v.i.
Ing. Jan Medřický, Ph.D. Oddělení materiálového inženýrství, Ústav fyziky plazmatu AV ČR, v.v.i.

Abstrakt: Prášky se sférickými částicemi se využívají v mnoha průmyslových odvětvích, například ve zdravotním, potravinářském nebo při aditivni výrobě, díky jejich vylepšeným tokovým vlastnostem. Sferoidizace plazmovým stříkáním je efektivním nástrojem pro výrobu takových prášků z ostrohranných nebo aglomerovaných prášků díky možnosti zpracovat velké množství vstupního materiálu v krátkém čase. V této práci byl popsán proces tvorby sférických částic, chování částic v horkém plynu a několik metod charakterizace prášků. Byla vyvinuta záchytová komora pro sferoidizaci prášků pomocí vysokoentalpického hybridního vodou stabilizovaného plazmového hořáku (WSP-H) s důrazem na maximální záchytovou účinnost. Byly provedeny sferoidizační experimenty s prášky Al_2O_3 a TiC a byla pozorována jejich morfologie, sfericita, tekutost, velikost částic a chemické a fázové složení. Bylo dosaženo úspěšné sferoidizace prášku Al_2O_3, což vedlo ke zlepšení jeho tekutosti. Zároveň bylo fázové složení výchozího prášku ovlivněno pouze minimálně. Při sferoidizaci prášku TiC došlo ke značnému zjemnění výchozího materiálu a k oxidaci na TiO_2.

Klíčová slova: atmosférické plazmové stříkání, sferoidizace, tekutost, fázové složení, obrazová analýza.

Title:
Morphological and Structural Changes of Ceramic Powders during Plasma Spraying

Author: Bc. Jonáš Dudík

Abstract: Powders with spherical particles are utilized in various industries such as health, food, or in additive manufacturing due to their enhanced flow properties. Plasma spray spheroidization is an effective tool for manufacturing of such powders from angular or agglomerated powder feedstocks, namely thanks to its high feedstock throughputs. In this thesis, the formation process of spherical particles in hot gases, the in-flight behaviour of the particles, and several methods of powders' characterization were described. The collection chamber for powder spheroidization using the high-enthalpy hybrid water stabilized (WSP-H) plasma torch was designed and manufactured with emphasis on maximal collection efficiency. Spheroidization experiments with Al_2O_3 and TiC powders were performed and the morphology, sphericity, flowability, particle size, and chemical and phase composition of resulting powders were observed. Successful spheroidization of Al_2O_3 enhancing its flowability without significant phase changes was achieved. In case of TiC, significant refinement and oxidation into TiO_2 powder was observed.

Key words: atmospheric plasma spraying, spheroidization, flowability, phase composition, image analysis.

Table of contents

List of abbreviations and symbols

WSP-H	Hybrid Water-Stabilized Plasma Torch
APS	Atmospheric Plasma Spraying
IPP, CAS	Institute of Plasma Physics, Czech Academy of Sciences
GSP, WSP	Gas-stabilized/Water-stabilized Plasma torch
SEM	Scanning Electron Microscopy
BSE	Back-Scattered Electrons mode
SE	Secondary Electrons mode
XRF	X-Ray Fluorescence Spectroscopy
XRD	X-Ray Diffraction
EDS	Energy-Dispersive Spectroscopy
WDS	Wavelength-Dispersive Spectroscopy
FC	Front part of collection Chamber
RC	Rear part of collection Chamber

D_{p0}, D_p	diameter of original and spheroidized particle	[µm]
Δ_p	thickness of the particle shell	[µm]
P_{eff}	effective power of plasma torch	[kW]
t_{sph}, t_{sol}	spheroidization and solidification time	[s]
μ_p	viscosity of liquid particle	[Pa·s]
V	volume	[μm^3]
σ_p	surface tension of liquid particle	[N/m]
r, R	radius of particle before and after spheroidization	[µm]
d_v	mass median particle diameter	[µm]
ρ_p, ρ_g	density of particle / gas material	[g/μm^3, g/ml]
h_c	convective heat transfer coefficient	[W/(m^2K)]
$(C_p)_p$	heat capacity of particle material	[J/K]
T_i, T_g	initial particle temp. and surrounding gas temp.	[K]
T_m	melting temperature	[K]
ΔH_m	latent heat of fusion of particle	[J/g]
Δv	difference in velocity	[-]
A	projected area of particle	[mm^2]
ρ_{rough}	perimeter of particle	[µm]
D_n, Dv (10), Dv (50), Dv (90)	percentile values in particle size distribution	[µm]

1 Introduction

Commonly, the plasma torch is used for preparing coatings or structures providing novel surface properties such as increased thermal, wear, or corrosion resistivity, which are hardly, if at all achievable by conventional bulk materials. These unconventional materials are prepared from, e.g., powders or liquid feedstocks [1, 2]. When a feedstock is injected into a plasma jet, it is dragged by its flow and the solid material is melted. The droplets then hit the substrate and solidify in a form of so-called splats. However, when the substrate is not present, the molten particles solidify in air at a certain distance from the jet, as their temperature decreases below the melting point of the material. Due to the surface energy of the liquid droplets of the molten material, the single particles form spheres in the air, resulting in spherical solidified particles. This process is thus called spheroidization. In general, spherical powders are often required for processes in health or food industry [3]. Also, for recently fast developing additive manufacturing, the spherical powders are required to ensure their smooth flowability as the powders often need to be spread evenly and melted layer by layer [4]. In this work, systematic development of the spheroidization process was carried out, including designing of a powder collecting apparatus, and two case studies using ceramic powders.

In the literature review of this thesis, the process of particle's spheroidization is described along with several spheroidization methods and their characteristic features. For instance, if the spraying is carried out in the open atmosphere (i.e., air), oxidation of certain materials sensitive to oxygen may take place. In addition, the main methods of powder characterization, such as flowability, particle size measurement, and chemical and phase composition will be described.

Experimental part of this thesis comprises of two tasks. In the first task, a new powder spheroidization chamber was developed for hybrid water/argon-stabilized plasma torch (WSP-H). The main objective was to achieve maximal powder collection efficiency. In the second task, the developed chamber was used for spheroidization of Al_2O_3 and TiC powders. The collected powders were analysed in terms of particle size and morphology, flowability, phase composition and chemical composition.

2 Theoretical part

2.1 Formation of spherical particles in plasma jet

When a particle or droplet (in case of suspension/solution feedstock) is injected into a plasma jet, it undergoes up to three processes: 1) heating of the particle or droplet, 2) melting of the solid phase, 3) evaporation of the melted material [5]. During the spheroidization process, molten droplets tend to form spheres in order to minimize their surface area.

Besides the dense spherical particles without any internal voids, hollow spheres are also frequently produced. The process of forming the hollow sphere is shown in Figure 1. When a porous particle (e.g., an agglomerate of very fine powder from a suspension) is injected into a plasma jet, the material starts to melt from the outside and forms a liquid shell. The shell prevents the gas entrained within the particle's internal structure from leaving the particle. The gas then forms a cavity (one or multiple) surrounded by the melting material. The size of the central cavity depends, for example, on the material's porosity, or the actual temperature of the particle, as the trapped gas expands with increasing temperature [6].

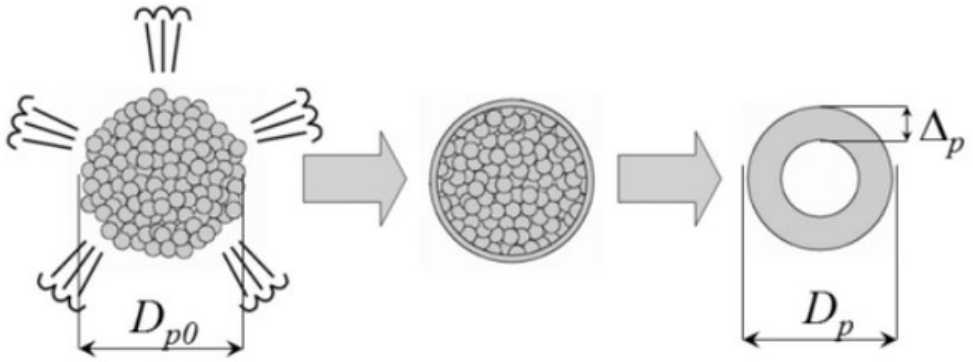

Figure 1: Schematic representation of a hollow sphere formation. D_{p0} and D_p denote the size of the original and spheroidized particle respectively, Δ_p denotes the thickness of the material shell [6].

Occasionally, donut-shaped particles can be formed. When the heating rate is high, evaporation of particle material can form a vapour bubble which then collapses and breaks through the particle, forming its donut shape [7]. Alternatively, in [8], Zhang et al. suggested another course of creating the pores inside the particles while using atmospheric plasma spraying (APS). According to Zhang, the pores originate from the rotation of the particles given by the rotating gas flow of the plasma jet.

Although the hollow spheres can be perceived as the defective, they can also be beneficial for some applications. For instance, hollow spheres have low density, low thermal conductivity, and high specific surface area [8]. Therefore, such particles are used as fillers in composite materials for its low weight and isolating properties [6]. Hollow

spheres can be also used for the production of thermal barrier coatings as the voids in the spheres increase the coating porosity, which is crucial for lowering the thermal conductivity of such coatings [8].

During the in-flight solidification of the droplets, crystallization of the material usually takes place, often forming a distinctive dendritic structure on the surface of the particles [9]. Also, cracking of the droplets is quite common if the excessive internal stresses are developed. Other phenomena potentially involved in the spheroidization process are decomposition of the original feedstock due to excessive heat, chemical reactions of the feedstock with the surrounding atmosphere (e.g., oxidation), or phase transformations [10].

2.2 Methods of spheroidization

There are several methods of spheroidization of powders. They generally differ in the form in which the feedstock material is delivered, and source of mechanical and thermal energy imposed onto the particles to form micrometre-sized particles. A few of them, such as spray drying, templating, and high-temperature remelting spheroidization will be described in following paragraphs. Basic principles of the methods and their benefits and disadvantages will be described in order to compare them to the spheroidization using atmospheric plasma spraying.

2.2.1 Spheroidization using atmospheric plasma spraying

Atmospheric plasma spraying provides a possibility to spheroidize particles with high melting point such as Al_2O_3 or ZrO_2 ceramics [8]. Using plasma as the heat source enables to process high loads of powders in a short time up to tens of kilograms of powders per hour [11]. According to Zhang et al., power of the plasma torch plays an important role in determining the size distribution of the spheroidized particles [8]. Therefore, the difference between spheroidization using gas-stabilized plasma torch (GSP) or water-stabilized plasma torch (WSP) can be significant. Both types of the torches were described in previous works [12, 13]. Briefly, the difference between the GSP and WSP torches is in the manner of stabilization of plasma inside the plasma chamber and in the source of the plasma-forming gases. The WSP torch is able to provide higher enthalpy and temperature, which can be as high as 28 000 K compared to 16 000 K in case of GSP torch [12]. Benefits of both technologies are merged in WSP-H technology [14].

The use of both, GSP and WSP, torches for spraying powders, which were then collected for further examination, was studied by Espie et al. in [11]. The authors used GSP torch with an effective power $P_{eff} = 18\ kW$ and WSP torch with $P_{eff} = 139\ kW$, resulting in a difference of plasma temperatures of about 10 000 K. For GSP torch, the iron particle collection was provided by a water-cooled cylindrical vessel in a vertical position. It was 650 mm tall and it had 130 mm in internal diameter. The entrance to the

vessel was only 16 mm in internal diameter and the entering particles were cooled by argon jets at the chamber inlet. The same apparatus could not be used for the higher enthalpy WSP torch due to the higher temperature of the plasma. Therefore, the iron particles sprayed by WSP torch were collected in liquid nitrogen. The plasma torch was oriented vertically, and the particles were sprayed into the collecting vessel. Such set-up was described for example in [8]. However, this method of collecting spheroidized particles is not preferable, especially for industrial setups, as the heat from the torch is rising and, therefore, can cause damage to the torch or to the injection nozzles during long-term continuous operation. Moreover, for some applications, the material shall not come in contact with water or liquid nitrogen. Prospective contamination by nitrogen, however, is hardly evitable as the majority of nitrogen contamination reportedly comes from atmospheric nitrogen [15].

2.2.2 Spray drying

Spray drying is commonly used not only for the spheroidization of powders, but also as a powder preparation process for forming of bigger powder particles from the smaller ones. During spray drying, the liquid material, i.e., emulsion, solution, or suspension, is atomized (i.e., disintegrated to droplets) by the atomization nozzle into a chamber, where it crosses a stream of a hot gas (Figure 2, a). The material can be either metal, ceramic, or composite [16]. As the liquid containing the material is injected into a stream of the gas, the liquid carrier evaporates, and spherical particles are formed and collected [17]. Even though spray drying can be used for spheroidization of powders, this method is rather expensive and time-consuming. In addition, the resulting particles are not sufficiently spherical and various shapes can occur as they usually do not reach the melting temperature of the original material, which demands a subsequent separation of spherical particles [8]. Also, the spray dried particles may be rather soft as the forming (nano)particles are merely stuck together after the solvent evaporation without strong bonding, which may deteriorate the powder's flowability. Similar process of powder preparation and spheroidization is called gas atomization. This process differs from spray drying by mean of atomization. While the atomization in spray drying is carried out by the atomization nozzle, in gas atomization it is carried out by a high-velocity gas crossing the stream of liquid material [18].

2.2.3 High-temperature remelting spheroidization

If only dense spheres are demanded (e.g., for metal additive manufacturing), the novel process called high-temperature remelting spheroidization can be used (Figure 2, b). During high-temperature remelting spheroidization process, the irregular particles are introduced into a high temperature region created by an electric heating furnace, where they melt and fall into the low temperature region, where the material solidifies as the spherical particles. The process takes place entirely in the atmosphere of

reducing gas, such as Ar and H_2 or CO, which reduces the oxides of the metal elements. Therefore, high quality spherical powders can be prepared with this technology [4].

2.2.4 Templating

Another method of creating spherical powders is called templating or nanocasting (Figure 2, c). Using this method, very precise hollow spheres can be prepared. A template consisting of micrometre or submicrometre sized cores is covered iteratively by a, for example, metal oxide material. Afterwards, calcination can be used to remove the template and to strengthen the hollow spheres. Materials such as carbon or silica can be used as a solid template. Using these materials, the textural properties of the hollow spheres can be enhanced, and the size of the pores can be controlled [19]. However, this method is also very costly and time consuming [8].

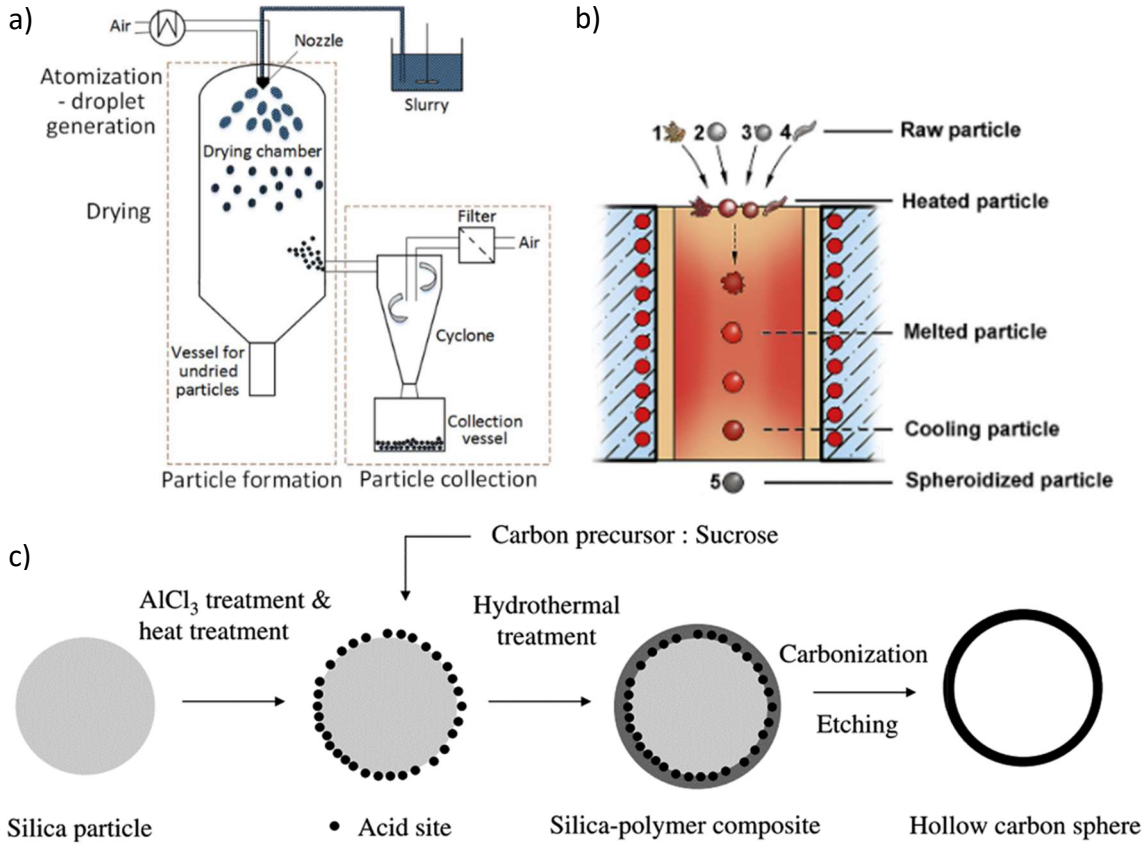

Figure 2: Schematic representation of spheroidization methods. a) spray-drying [16]*, b) high-temperature remelting spheroidization* [4]*, c) templating* [20].

2.3 In-flight oxidation and decomposition of particles

Particle oxidation is a common phenomenon in thermal spraying in open air [11]. Due to high velocity of plasma jet and the eddies around the jet, air atmosphere consisting primarily of nitrogen and oxygen is inevitably entering the plasma. The presence of the oxygen together with high temperature of the plasma result in oxidation of the oxygen-sensitive materials. Particularly, three stages of particle oxidation occur: transport of the oxidizing agent from the surrounding atmosphere to the particle, chemical reaction of the oxidizing agent with the surface of the particle, and diffusion of oxygen into the particle [21]. Thus, their composition and melting properties are changed. Oxidation may generally take place during both, in-flight stage as well as after the deposition of the splats in case of coating deposition. These changes influence the resulting coatings as well as the powders which are processed/spheroidized by plasma spraying.

The degree of oxidation of the particles can be measured either by chemical separation and weighting the oxides or analytically by calculation of the oxygen content based on the measurements of oxides provided by, for example, X-Ray diffraction [21, 22]. Espie et al. reported, that in case of GSP torch, the oxidation appeared on the particle surface as well as inside the particles in a form of so called “nodules”. On the contrary, while the WSP torch was used, the nodules were not present, but the oxidation crust on the surface of the particles was much thicker. The main reason of the thicker oxide crust in case of the WSP torch is not only higher enthalpy of plasma, but also the longer jet, thus the longer flight time of the particles, so that the oxidation layer has more time to grow.

The in-flight oxidation during APS process can by partly prevented by a combustible gas shrouding the plasma jet [11]. Shrouding by nitrogen-hydrogen mixture or by acetylene was carried out, for instance for spheroidization of steel powder, by Voleník et al. in [15]. Acetylene shrouding turned out much more effective (4 – 5 times) as the oxide layer on particles was significantly thinner when compared to nitrogen-hydrogen shrouding. While nitrogen-hydrogen was used, the oxidic scale was thicker with pronounced dendritic growth. This was caused by acetylene working not only as a barrier between atmosphere and the plasma plume as in case of nitrogen-hydrogen, but the oxygen from the plume was also consumed by acetylene burning. Shrouding was successfully used also for preparing tungsten coatings by Matějíček et al. in [23]. In addition, according to Kambara et al., the size distribution of a feedstock powder also significantly affects the degree of oxidation. It was reported that a narrow size distribution of a raw powder without nano-sized particles leads to mitigation of oxidation while using plasma spraying. The increase of oxidation in case of broader size distribution is reportedly caused by presence of small particles [24].

High temperatures reached in plasma can lead to decomposition or change in stoichiometry of some materials, such as bioceramics [25]. High enthalpy of plasma is consumed by the material as a driving force of the decomposition. The use of suspension feedstock can slightly mitigate this phenomenon, as the enthalpy is primarily absorbed by the liquid carrier [26]. Due to the high temperatures, most of the organic polymers cannot be processed by plasma spraying, as the plasma thermal energy is high enough to break the primary chemical bonds, thus effectively destroying the polymeric chains [27].

2.4 Collection of the particles

The spheroidized powder is generally collected in a vessel or chamber. In the process, multiple technological parameters have to be considered and optimized, for example, plasma temperature, particle velocity, trajectory, and feeding rate, shape and size of the vessel, or turbulences in the flow of the particles. Beckers et al. in [28] studied the behaviour of particles spheroidized in a chamber using gas atomization. The general profile of velocities of the particles can be seen in Figure 3, a, b). The particles are accelerated to maximum velocities when they are injected into the stream of gas. Then, part of the particle stream turns back and accelerates to similar velocities in the opposite direction. Back on the front end of the vessel, the stream is again torn down in the primary direction, but a part of the stream is pulled into the entrance throat (Figure 3, b), where it can be either turned back again or it can even leak from the chamber. The gas recirculation in the chamber causes collisions of the particles (Figure 3, c). Generally, as the smaller particles solidify earlier than the larger ones, they may stick to the large liquid particles when they collide, thus forming so-called satellite particles [24]. Therefore, the conditions in the chamber can lead either to good sphericity of the powder as well as to the collisions between the particles resulting in their deformation and agglomeration. These conclusions may be applied on any kind of spheroidization set-up involving a closed or partly closed vessel.

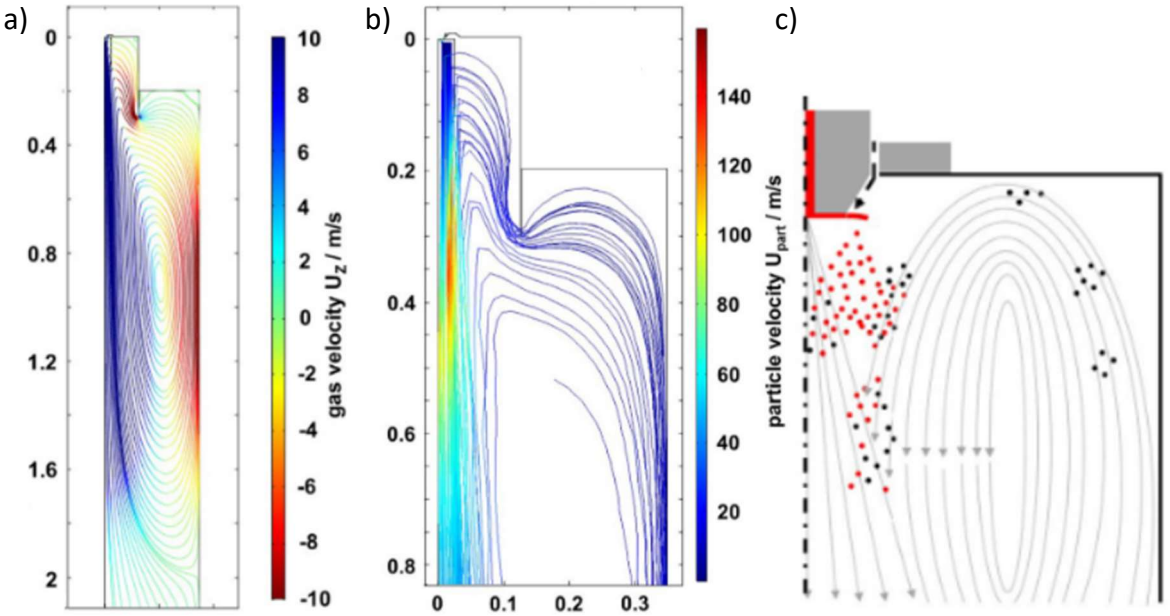

Figure 3: Cross section of the gas atomization chamber. a) The velocities of the particles in the chamber, b) the detail of the upper part of the chamber, c) the formation of satellite particles [28].

2.5 Spheroidization time

Another factor in spheroidization affecting the sphericity of the particles is the spheroidization time, which must be shorter than the solidification time [28]. Spheroidization time refers to the time needed for surface tension forces to create a sphere from a molten particle, and it is given by

$$t_{sph} = \frac{3}{4}\frac{\pi^2 \mu_p}{V\sigma_p}(R^4 - r^4), \tag{1}$$

where μ_p is viscosity of the liquid particle material, V is the volume of the particle, σ_p refers to the surface tension of the liquid particle, R is a radius of the particle after transformation to spherical shape and r is the radius before the transformation to spherical shape.

The formula for calculating the solidification time composes of two parts. One part represents the time for cooling the liquid material to its melting temperature, the second part refers to the time needed for the particle to lose its latent heat of fusion. The solidification time can then be written as follows:

$$t_{sol} = \frac{d_p \rho_p}{6h_c}\left[\left(C_p\right)_p \ln\left(\frac{T_i - T_g}{T_m - T_g}\right) + \left(\frac{\Delta H_m}{T_m - T_g}\right)\right], \tag{2}$$

where d_p is a mass median particle diameter, ρ_p is a density of the particle material, h_c is a convective heat transfer coefficient, $\left(C_p\right)_p$ refers to a heat capacity of the particle

material, T_i is an initial temperature of the particle, T_g is a temperature of surrounding gas (or plasma), T_m is a melting temperature of the particle material, and ΔH_m refers to the latent heat of fusion of the particle. If the spheroidization time was longer than the solidification time, the particles would have resolidified in various shapes.

During atomization, the size of a particle is determined by the maximum stability criterion, which is a function of the surface tension of the liquid particle and the maximum relative velocity between the liquid and the gas. Mathematically, the maximum stability criterion is given by

$$\frac{1}{2}\rho_g(\Delta v)^2 = Const.\frac{\sigma_p}{d_p}, \tag{3}$$

where ρ_g is the density of gas and Δv refers to the difference between the velocity of particle and the gas. The constant depends on the conditions of acceleration and the type of flow [29].

2.6 Particle's characterization

The success rate of the spheroidization depends not only on the collection efficiency of the powder, but also on several particle characteristics. These are crucial for determination of the quality of the treated powders as well as the repeatability of the spheroidization process. Some of the characteristics and the methods of testing them will be described in following paragraphs, including flowability, particle size, and chemical and phase composition.

2.6.1 Flowability

The ability of a powder to flow without clogging or pulsation, so called flowability, is crucial for many manufacturing technologies, such as powder-based additive manufacturing. For thermal spraying in particular, the powders need to flow smoothly through the feeders to the plasma jet [4]. Especially when fine powders are used as a feedstock material, clogging of the feeder nozzles becomes a frequent problem [30]. Besides thermal spraying, other industry processes may also require good flowability of powders to prevent their clogging in hoppers or silos, etc. Such an event can cause unwanted interruption of the process, in which the powder is used. Also, partial powder clogging can also induce a temporary variation in powder feeding rate, which is delivered from the hopper or the tube [31].

Sometimes, the simplistic view on flowability can refer to it as a characteristic on a scale from free-flowing to non-flowing [3]. However, as flow behaviour of a powder depends on multiple powder characteristics, the same powder can, for example, flow through one type of a hopper while struggling to flow through another. Therefore, a more complex view on this property is often required [3].

To ensure a good powder flowability, an appropriate particle size distribution, high degree of sphericity, and low moisture content are required. When spheroidizing the powders with plasma spraying, the size distribution is an important factor as the flowability is also negatively influenced by the presence of satellite particles, which can attach to the larger particles in a plasma flow. Formation of such particles can be avoided by lowering the concentration of the particles in the flow, thus reducing the possibility of particle collisions. Moreover, the reduced particle concentration may also lead to more spherical particles as the feed rate has a strong influence on heat transfer between the plasma and the particles. When the feeding rate is excessively high, the energy needs to be divided between more particles resulting in a lack of the amount of energy per one particle [32]. On the other hand, if available, an increase in torch power may compensate the potential lack of energy, and thus it should improve the spheroidization efficiency while preserving high feeding rates [5].

Usually, the term “flowability” is used for a couple of properties known as flow properties. The most important flow properties are cohesive strength, density, wall friction, and permeability. Cohesive strength refers to ability of the powder to retain its shape as, for example, sandcastle. Unlike the bulk material, the bulk density (or compressibility) of a powder is rather a variable than a single value. When the powder flows through the hopper, with the increasing wall friction, the hopper wall must be steeper to ensure a proper flow. The finish of the wall surface and its angle have, therefore, significant influence on the flowability through a hopper as well. A permeability is the ability of the powder to allow air to pass through it. It can be used to calculate a critical discharge rate of the powder from the hopper at which flooding (i.e., clogging with a high amount of powder) occurs. Such information can then be used to optimize a hopper design. When pressure is applied on the powder, a flow resistance increases, so that the powder flows less easily. Based on that, one possibility of determining the flowability is so-called flow function. The flow function is given by the relationship between the consolidation pressure and the cohesive strength. An example of two flow functions is shown in Figure 4 [3]

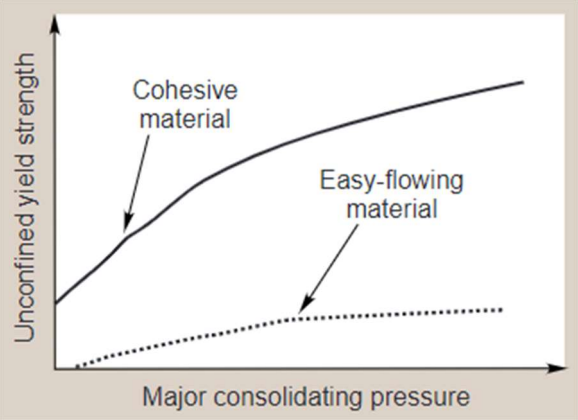

Figure 4: An example of a flow function [3].

In thermal spraying, several problems can occur while feeding the powder. When a powder with high cohesive strength flows through a simple hopper, two types of disorders can occur, an arch or a rathole. An arch refers to a stable obstruction formed in the hopper usually near its outlet. The arch then blocks the rest of the hopper content from discharging. A rathole is a cavity emptied above the hopper outlet, while the surrounding content stays inside. A collapse of a rathole in fine powder can result in flooding, which means an uncontrollable flow through the equipment. On the other hand, fine powders may also suffer from opposite problem, when the expansion of the inside voids creates upward air pressure gradients [3].

These problems are strongly affected by a pattern of the flow through the hopper. The two typical flow patterns, a funnel flow and a mass flow, are shown in Figure 5. In funnel flow, a large rathole usually occurs, while in mass flow all powder is in motion. To

achieve a mass flow, an appropriate size of the outlet as well as the properly steep and smooth walls of the hopper are required [3].

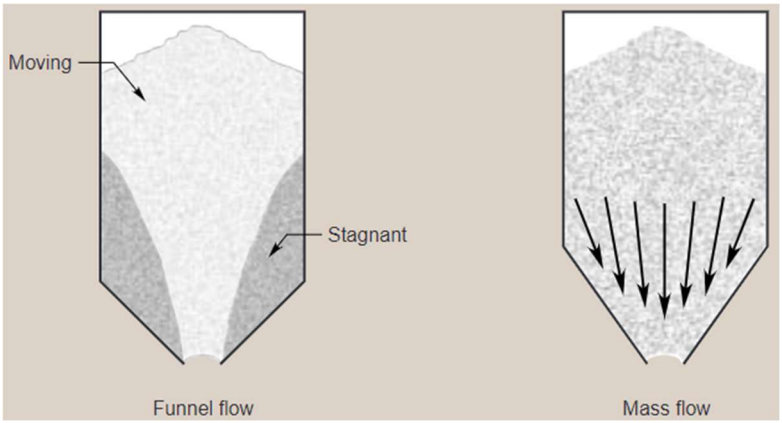

Figure 5: Flow patterns of a powder in a hopper [3].

2.6.1.1 Flowability testing

One of the simplest methods of testing a flowability is using a Hall flowmeter according to ASTM B213 standard [33]. A Hall flowmeter is a funnel of a defined dimensions and material with an orifice of 2.54 mm or 5 mm in diameter (see Figure 6). To start the test, 50 g of powder is poured into a properly clean funnel, while the orifice of the funnel is blocked by a clean and dry finger. The finger is removed from the orifice simultaneously with a start of a timer. The powder should start to flow out of the funnel spontaneously. If the powder fails to start flowing, one light tap on the funnel is permitted. A timer is stopped at the moment when the last powder seed is emptied from the funnel. More than one test run with a fresh 50 g of powder should be proceeded to obtain representative statistics. Another version of the flow test is possible, in which an orifice is not blocked by the finger and the timer is started simultaneously with a start of pouring a powder into a funnel. However, some powders may not flow through the funnel properly. This occurs especially with very fine powders, lubricated powders, and wet or moist powders. When a powder does not flow through a Hall flowmeter, the Carney flowmeter funnel can be used in accordance with ASTM B964 standard. When spheroidizing powders, the method provides a possibility to compare flowability of the spheroidized powder to the raw powder. Generally, the flowability value of the powder with spherical particles should be increased.

In addition, Hall flowmeter can be used to measure apparent density of the powder. Sufficient amount of powder is poured into a funnel and collected as it flows through into a collector of standardized volume. According to ASTM B213, the volume of the collector should be 25 cm^3 [33]. When the collector is full of powder, the excess piled-up powder is scraped off and the powder level is aligned with the top of the collector. Full collector is then weighed and the weight of empty collector is subtracted from the weight

of full collector. The apparent density of the powder is then calculated as the powder mass divided by its volume.

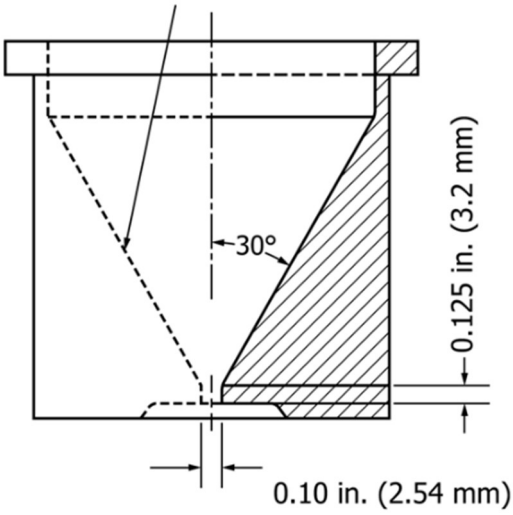

Figure 6: Scheme of Hall flowmeter funnel [33].

2.6.2 Particle size and morphology

Particle size is another important parameter which needs to be measured while characterizing a powder. When spheroidizing a powder by plasma spraying, it is important to measure the particle size (a diameter or a volume) of raw feedstock powder as well as that of a powder which was processed by plasma torch. During the spheroidization process, single particles can be partially evaporated, broken into smaller particles or, vice versa, they can merge into larger particles. The particle size can be determined by several methods. The powders can be analysed by a sieve analysis described in ASTM B214 standard. A group of sieves is placed one on another with descending size of their openings. The coarsest sieve is at the top. The powder is placed on the top sieve and a sieve assembly is fastened in a sieve shaker. The shaker then operates for a given time (15 minutes according to the standard). The amount of powder in each sieve is weighed and the particle size distribution is evaluated [34].

X-Ray absorption or laser light scattering particle size measurement devices are significantly more accurate and, unlike the sieve analysis, it is usually possible to measure the particle size of dry powders as well as for powders dispersed in a suspension. A beam of light or X-ray is scattered as it passes through a powder sample. The system of the particle analyser uses the measured intensity profile of the scattered beam to calculate the size distribution of the particles. There are several theories used in laser-based particle size measurements which characterize the interaction of the particles with the beam of light. The Lorenz-Mie theory is derived from Maxwell's equation solution which describes scattering of the light by a homogeneous sphere. The Fraunhofer theory is the large particle approximation of the Lorenz-Mie theory. Unlike the more precise Lorenz-Mie theory, knowledge of optical properties of the particles as well as that of the

dispersant is not required in Fraunhofer theory. The other theory, Rayleigh theory, is usable for particles with the diameter significantly lower than the wavelength of the scattered light only [35, 36].

Typically, the size distribution of the particles is displayed under the designation $d_n = x$, which means that n % of particles is smaller than x. Two types of size distribution are possible to be displayed, a volumetric and a number size distribution. In number size distribution, each particle is included in the distribution with the same weight. In volumetric size distribution, the particles are included with a weight according to the volume of each particle [37].

When measuring the particle size, increased attention needs to be paid to the selection of the tested samples, i.e., to the sampling of the powder. Two sampling errors can be distinguished: errors due to segregation of the powder and statistical errors [38]. For example, when the powder is stored, larger particles can sediment in the bottom of the container, so that the sample taken from the top does not represent the whole [2]. The sedimentation can also occur during the manufacturing the powder [38]. Therefore, each container with the powder should be worked up before the sampling, or, if needed, use of some sampling method, as, for example, in [38] should be considered. The statistical errors due to random fluctuations, on the contrary, cannot be prevented [38].

2.6.2.1 Image analysis

The particle size can be also measured using scanning electron microscope (SEM) [2]. The micrographs of loose powders are processed by image analysis, which is able to evaluate morphological characteristics of individual particles. However, in order to observe the internal morphology, i.e., for example, porosity, metallographic preparation of cross-sections is required. When determining the size of irregular particles, multiple dimensions is needed to be measured. However, the derived diameters such as Heywood equivalent diameter are usually used. The Heywood equivalent diameter is the diameter of a circle with the same area (in the 2D image) as the original particle [39]. When acquiring the information about circularity (or sphericity) of the particles using image analysis, two approaches are possible. Circularity can be calculated from the distance between pairs of parallel tangents to the projected outline of the particle in selected fixed direction, or it can be calculated according to formula giving the so-called Cox circularity,

$$Circ. = \frac{4\pi A}{p_{rough}^2}, \tag{4}$$

where A is a projected area and p_{rough} is a perimeter including roughness measured by pixel counting. The Cox circularity is, however, affected by the so-called “Coastline of Britain problem”, which is caused by the resolution of the image. Another shape

characteristic of the spherical particles can be obtained as a ratio of the minor axis and the major axis [39].

2.6.3 Chemical and phase composition

Another important powder characteristics is its chemical composition. Moreover, as the temperature changes quickly with the distance from the plasma torch during the plasma spheroidization, the cooling rates of the molten particles are very high. The high cooling rates lead to formation of supersaturated solutions, and thus various unconventional metastable phases may be produced [40]. In this chapter, several methods of chemical and phase composition employing X-rays will be described. Two basic types of composition analysis may be distinguished. Qualitative analysis determines what elements or phases are present in the tested sample. Conversely, quantitative analysis determines how much of constituent is present in the sample. Reference data are nowadays usually included in the software library of an analysing device, so that the comparison of measured data with these reference data is evaluated automatically, and no additional measurements of reference samples are needed.

Chemical (elemental) composition can be relatively easily determined by X-ray fluorescence spectroscopy (XRF) or X-Ray photoelectron spectroscopy (XPS). Similarly to XRF, scanning electron microscopes (SEM) can also bring the information about chemical composition as they can be equipped with similar detectors as XRF either for energy-dispersive spectroscopy (EDS), or wavelength-dispersive spectroscopy (WDS). The possibility of implementing these detectors into SEM is beneficial especially when micrographs of the samples need to be recorded as well as its chemical composition at microscopic scale. Information about phase composition of powder is usually provided by X-ray diffraction (XRD) technique. All these methods will be described in following paragraphs.

2.6.3.1 X-ray spectra

According to [41], X-ray can be defined as "*electromagnetic radiation in the wavelength region ~10^{-5}-10 nm produced by deceleration of high-energy electrons and/or by electron transitions to the inner orbits of atoms*." X-ray emission spectra consist of two contributions, continuous and characteristic (Figure 7). Continuous spectrum, also called "bremsstrahlung", originates from direction changes or slowing down of electrons due to inelastic scattering in the specimen and due to electric (Coulombic) field around the atom nuclei. Characteristic spectrum, also called line spectrum, composes of peaks at specific wavelengths or energies.

To obtain a proper quantitative analysis, i.e., to identify a quantity of each element present in the tested sample, continuous part of spectrum needs to be subtracted from the characteristic part of spectrum. The subtraction is made by measuring the intensity of continuous spectrum in places, where no peaks from

characteristic spectrum are present. The measured intensity values are then interpolated into the non-measured places. Therefore, the whole continuous spectrum is marked by a line and can be subtracted easily [42].

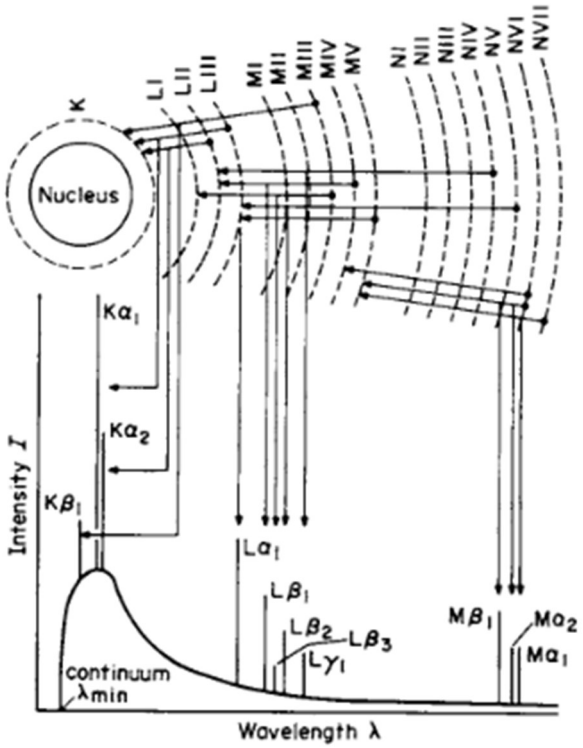

Figure 7: X-ray spectra and atom's orbital shells [41].

2.6.3.2 X-ray fluorescence spectroscopy (XRF)

The chemical composition of a tested sample in terms of presence of elements with atomic number typically higher than 11 in the sample (either powder, compact bulk material or even liquid) can be determined by XRF method [43]. When primary high energy X-ray emitted usually from a controlled X-ray tube hits the sample, an electron is dislodged from one of the atom's inner orbital shells. An electron from higher energy orbital shell fills the vacancy in lower energy orbital shell and its energy is lowered by releasing a fluorescent X-Ray. This X-ray is processed by monochromatizer and measured by a detector and the origin element is determined, as each element produces unique characteristic fluorescent X-ray spectrum. Two types of analyses can be used in XRF, energy-dispersive (EDS) and wavelength-dispersive (WDS) [41, 44].

2.6.3.3 Energy-dispersive (EDS) and wavelength-dispersive (WDS) analyses

Unlike the WDS, in EDS monochromatization before the detection takes place according to its energy, while in WDS it takes place according to the wavelength. Using EDS, the acquisition is relatively fast and easy and whole spectrum is displayed almost at one time, but, on the other hand, the resolution is lower than that of the other techniques. Thanks to the fast acquisition, X-ray mapping is also possible in SEM. With X-ray mapping, the elements present in the sample can be displayed on the micrograph

over the spot, where they were detected. Single element maps can be displayed as well as composed map with all detected elements (Figure 8) [44].

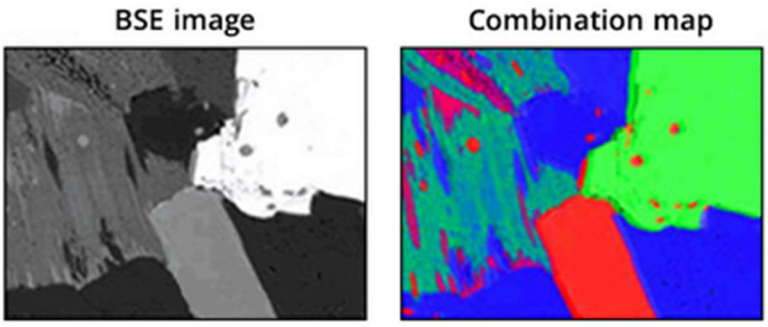

Figure 8: An example of X-ray map [44].

2.6.3.4 X-ray diffraction (XRD)

Previously described methods can provide the information about the chemical composition of a tested sample. When additional microstructural features are desired to be known, such as phase composition, crystalline sizes and their orientation, and presence of the defects and microdefects as, for example, voids, second phases, or dislocations, other methods need to be used. These techniques are based on diffraction which can refer to waves associated with electrons (selected area diffraction – SAD or electron backscatter diffraction - EBSD), or to X-rays (XRD), which will be described in this paragraph [2].

Similarly to the previous methods, the data from the XRD compose a spectrum. However, in case of the XRD, the spectral peaks do not show elements, but crystalline phases [2]. The phases in the lattice are represented by characteristic peaks. The height of a single peak is then given not only by a quantity of the present phase, but also by various parameters as follows: structure factor, multiplicity factor, Lorentz-polarization factor, absorption factor, temperature factor and unit cell volume [1, 45].

When the data is collected from a material and the spectrum is acquired, it needs to be translated into the requested information, i.e., quantitative and qualitative analysis. Firstly, the percentage of amorphous phase is calculated using the measuring of a background. Then, the analysis of single peaks follows [2, 45].

The most used method of quantitative analysis in powder diffraction is the Rietveld method. It can be applied either on multiphase samples as well as single phase. Each peak of the spectrum has almost exactly Gaussian profile reflecting several parameters such as sample shape or sample crystallinity. Taking into account other factors, such as absorption of X-rays by the sample, the peak shows a slight asymmetry. However, with several approximations of peak shape and other factors, for example, the structure factor, and sample characteristics, the parameters for least squares method can be determined. The least squares refinement is then performed to fit experimentally

measured data, which are then interpretable for quantitative phase analysis. For the Rietveld quantitative analysis, the database of crystal structures is needed to provide all the required data [42, 46, 47].

3 Motivation – past experiments at IPP, CAS

Several experiments with spheroidization of powders using plasma torch were previously carried out at Institute of Plasma Physics, CAS (IPP). Two basic setups, “dry” and “wet”, were generally used as initial experiments.

- In experiments with the dry setup, the particles were sprayed with the torch without any particular collecting facility and the resulting powder was collected from the exhaust funnel of the spraying room, where the powder settled down. The powder was thus collected approximately 1.5 m away from the torch. Another method of collecting the powder in dry experiments was using a stainless steel “pot” placed at the distance of about 500 – 600 mm in front of the torch.
- Wet setup involved collecting the powder into a container filled with liquid placed below the torch positioned vertically towards the container. Inside, water, mixture of water with 10 % of ethanol, or liquid nitrogen were typically used for immediate cooling of the sprayed feedstock. The distance of the torch from the liquid level was 300 – 500 mm. Spraying with inclined torch into liquid was also tried, but in such case, the particles tended to rebound from the liquid surface.

Both dry and wet experimental setups involved certain disadvantages. Collecting of the powder from the exhaust funnel of the spraying room was sufficient only for observing sphericity of the powder after the spraying. However, further characterizations such as chemical and phase composition or flowability testing were not possible due to contamination of the powder with other, previously sprayed powders as well as other impurities.

Collecting the powder into a liquid is unsuitable for the powders which should not be in contact with the liquids. Moreover, when a powerful torch, such as the water-stabilized or hybrid water-stabilized plasma torch are used, the heat rises around the body of the torch and can potentially cause severe damage to the equipment.

Based on the knowledge from previous experiments, first version of a collecting chamber was designed couple of years ago (Figure 9 and 10) in order to provide repeatable and reliable collection of the processed powders without the risk of contamination thereof and/or equipment damage. A steel tube of about 41 cm in diameter and 100 cm in length was used as the collector. The dimensions of the tube were limited by the space available in the spraying room as a longer tube would not fit between the plasma torch and the exhaust funnel. In the front and in the rear ends, there were attached metal sheets reaching up to roughly one third of the tube’s diameter. The sheets were supposed to prevent the powder from escaping the chamber. In the frontal section of the tube, two cooling holes were made to allow the heat delivered by the torch to escape sideways out of the chamber (see Figure 9 and 10). Finally, there was an

oblique metal sheet inside the tube serving as a partition. The sheet was intended to deflect the particles' trajectory in order to prevent the powder from escaping the chamber straight forward with the stream of the gas. In addition, spraying experiments with argon, nitrogen or other reducing gas shrouding was attempted to minimize the undesired oxidation of oxygen-sensitive materials. Despite many drawbacks, this setup served as a basis for the development of the improved collection chamber in this work.

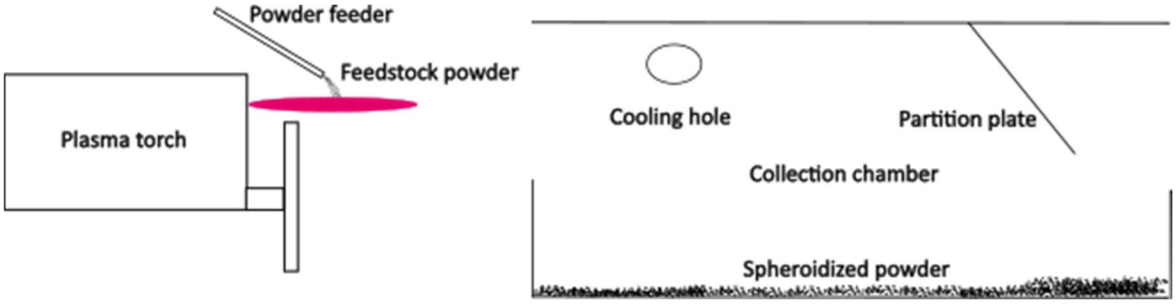

Figure 9: Schematic of the original spheroidization set-up used at IPP.

Figure 10: The original spheroidization setup used at IPP. Please note that the sample holder was not present in current experiments.

Two tasks were the main objectives of the experimental part of this thesis: to develop a collecting chamber for powder spheroidization experiments with maximal collection efficiency (at least 90 %) as task 1, and then to use this chamber for spheroidization experiments with model materials followed by their characterization and comparison of their properties as task 2.

4 Experimental

During development of the chamber, the attention was focused on ensuring high-temperature resistance during powder collection and easy manipulation, maintenance, and cleaning in order to avoid contamination of powders. Clay shale and Al_2O_3 powders were used for testing of the powder collecting efficiency, as they were readily accessible at the IPP. After the chamber was developed, Al_2O_3 powder was used in the first spheroidization experiments due to its interesting morphology, phase changes during plasma spraying and a long-term interest of the IPP in this material. Furthermore, two experiments with TiC powders were carried out on request of an industrial partner. All the plasma treated powders as well as the feedstock powders were observed using scanning electron microscope. The recorded micrographs of Al_2O_3 powders were used for the image analysis to evaluate particles' circularity and the presence of non-spheroidized particles. Subsequently, particle size distribution, flowability, apparent density, and chemical and phase composition of the powders were evaluated.

4.1 Materials and methods

4.1.1 Task 1 – Designing the collecting chamber and spraying parameters

The initial spray collection experiment was carried out in order to observe the benefits and shortcomings of the original collecting chamber (D1, Figure 10), in particular the collection efficiency of the chamber. A clay shale feedstock powder was fed into the plasma jet generated by the hybrid water-stabilized plasma system WSP-H 500 (ProjectSoft HK a.s., Czechia) using two volumetric powder feeders (Sulzer, Switzerland). The spraying was carried out in multiple cycles, between which the chamber walls were cooled. The initial spraying parameters were established according to the knowledge from the past experiments and were optimized along with the development of the chamber design (see Table 1).

Several step-wise changes in the chamber design were made according to the performance of each design. These included sealing of the original cooling holes in the front section as well as attaching lids at the front and the rear ends of the chamber. The front-end lid accommodated a circular opening (100 mm in diameter) as powder inlet and a 75 cm long chimney was attached to the rear-end lid in order to supress escaping of the airborne particles. Active cooling provided by two water misting nozzles was added above the chamber for more efficient heat removal. Moreover, the distance between the torch and the chamber inlet, i.e., spraying distance (SD), was also decreased after the first experiment (Table 1).

With the second iteration of the vessel, D2, Al_2O_3 powder Surprex AW24 (Fujimi, Japan) was sprayed (see Table 1 for spraying parameters) with the prospect of the following study focused on powder characterization. Also, two gravimetric feeders G4™

(Uniquecoat Technologies, LLC, USA) were used for introducing the Al_2O_3 powder into the plasma jet, as they, unlike the volumetric feeders, allow a precise control of powder feeding rate. With the knowledge of the amount of powder fed into the jet, the collection efficiency in percent was determined.

For the 3D design experiment, the partition was moved further away from the chamber inlet in attempt to minimize the coating build-up thereon.

In the final design of the collection chamber, D4, an attachment was added to the top of the vertical chimney (see Figure 11). The attachment was widening in order to slow down the particle flow and a steel mesh was placed inside to further decrease the flow speed and possibly even reflect the particles back into the chamber. The partition plate was also moved back to its original position and tilted so that the angle between the plasma flow and the partition plate was shallower, making the deposition of molten droplets less probable. The gaps between the components (namely the perimeter tube and front and rear lids) were sealed by Al_2O_3 felt liner which allowed thermal expansion of the whole device and prevented the powder from escaping through the narrow openings. The final design of the chamber as rendered in Solid Edge 2022 software and the photograph of the final chamber is shown in Figure 11. The diameter of the extended part of the chimney was changed according to the diameter of the steel mesh inside.

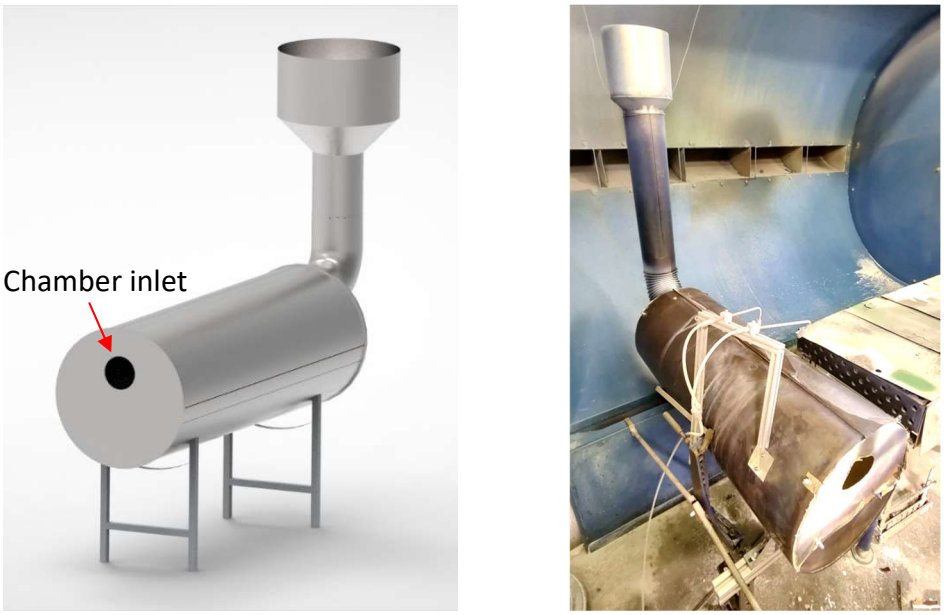

Figure 11: The final design of the collecting chamber rendered in Solid Edge 2022 software and its photograph.

Table 1: Spraying parameters used in design stage of collecting chamber development.

Experiment designation	**CS**	**A-SD250**	**A-SD150a**	**A-SD150b**	**A-SD150c**
Chamber designation	D1	D2		D3	D4
Material	Clay shale	Al_2O_3	Al_2O_3	Al_2O_3	Al_2O_3
Granulometry [µm]	-100+63	-75+38	-75+38	-75+38	-75+38
Repetitions of spraying cycles	4	6	6	6	16
Spraying time in each cycle [s]	30	30	30	30	30
Spraying distance (SD) [mm]	350	250	150	150	150
Feeding distance (FD) [mm]	35	45	45	45	45
Feeding rate [kg/h]	10	10	10	10	10
Chamber cooling	Air + holes	Water spray		Water spray	Water spray
Powder collection area	Front of the chamber	Front of the chamber		Front of the chamber	Front and rear of the chamber
Design modifications	Original	Cooling holes sealed; chimney added; inlet size decreased		Shifted partition	Tilted partition; chimney expansion; mesh in chimney
Schematic of the experimental setup	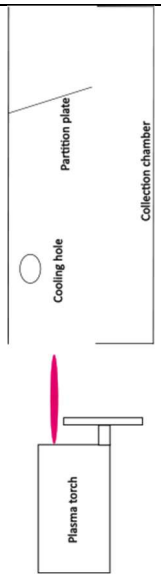	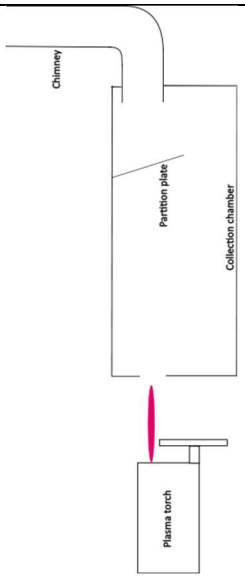		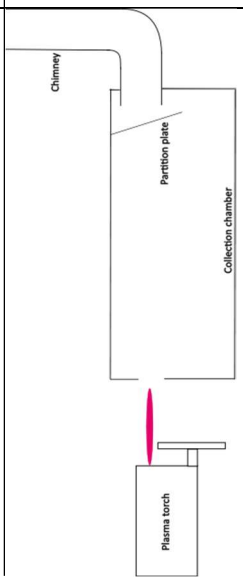	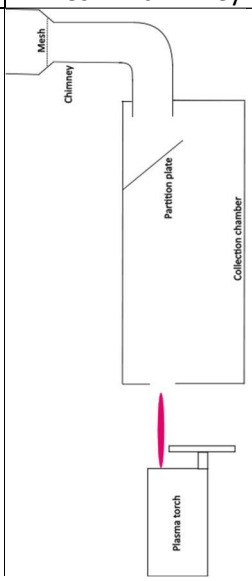

4.1.2 Task 2 – Spheroidization experiments

4.1.2.1 Preparation of powders

For spheroidization, WSP-H 500 (ProjectSoft HK a.s., Czechia) system was used. The feeding of powders was again provided and controlled by two gravimetric feeders G4™ (Uniquecoat Technologies, LLC, USA). The spraying was performed with the final collecting chamber design D4. Before each experiment, the collector was cleaned to eliminate the contamination of the collected powders. As feedstock materials, Al_2O_3 Surprex AW24 (Fujimi, Japan) and TiC Amperweld (Höganäs, Sweden) powders were used. Denomination of samples and the spraying parameters of spheroidization experiments are listed in Table 2. In case of A2x-SD150 experiment, the previously collected powder from A-SD150c experiment was used as a feedstock in order to evaluate the influence of repeated spheroidization of the powder. The Al_2O_3 powders were collected separately from the front part of the chamber and from the rear part in order to test homogeneity of the powders. The powders collected from the front and rear parts of the chamber were characterized separately and denoted as “FC” and “RC”, respectively.

For the spheroidization of Al_2O_3 powder, the parameters established in A-SD150a experiment were used. For the spheroidization of TiC powder, feeding rate was decreased from 10 kg/h to 5 kg/h according to the limited amount of powder available for the experiment and to prevent clogging of the feeding lines by the fine TiC powder. For the experiment with TiC, two different feeding distances (i.e., distance between the feeding nozzles and the plasma nozzle) were used (see Table 2).

Table 2: Spraying parameters of spheroidization experiments.

Experiment designation	**A-SD150c**	**A2x-SD150**	**T-FD45**	**T-FD120**
Material	Al_2O_3	Al_2O_3 (A-SD150c)	TiC	TiC
Granulometry [µm]	-75+38	~ (-75+38)	-45+5	-45+5
Repetitions of spraying cycles	16	8	3	3
Spraying time in each cycle [s]	30	30	30	30
Spraying distance (SD) [mm]	150	150	150	150
Feeding distance (FD) [mm]	45	45	45	120
Feeding rate [kg/h]	10	10	5	5
Chamber cooling	Water spray	Water spray	Water spray	Water spray
Powder collection area	Front and rear of the chamber	Front and rear of the chamber	Whole chamber	Whole chamber
Schematic of the experimental setup D4	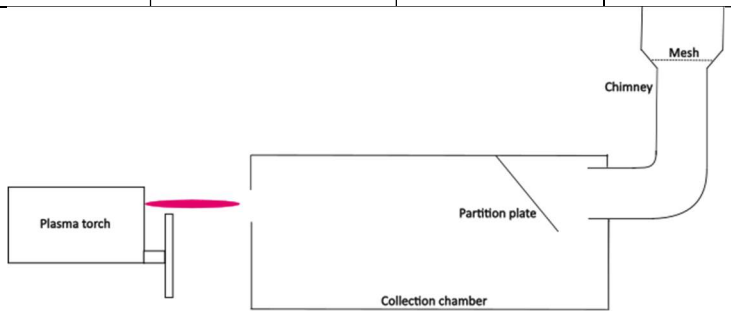			

4.1.2.2 Preparation and observation of metallographic samples

A few grams of each collected powder as well as the feedstock powders were embedded in low-viscosity epoxy resin (Epofix, Struers, Denmark). In order to ensure representative distribution of the powder particles in the metallographic samples, a two-step mounting method was used. First, a powder was mixed with low-viscosity epoxy and let cure. After curing, this piece was cut across employing high-speed precision saw Secotom-50 (Struers, Denmark) and the cross-section was cleaned in acetone and vacuum impregnated in the epoxy resin again. After the resin cured, the samples were grinded and polished using a semi-automated polisher Tegramin 25 (Struers, Denmark) with sandpaper and diamond suspensions according to the standard procedure used at IPP for ceramic samples.

Free surfaces of loose powders were also prepared for microscopic observation. Small amount of each powder was poured on adhesive conductive carbon tabs. A

compressed air was used to improve electrical contact and to remove the unstuck particles in order to avoid contamination of the microscope chamber by releasing not properly attached particles.

The observation of both free surfaces and polished cross-sections of powders was performed using an analytic high-resolution scanning electron microscope (SEM) Apreo 2 S LoVac (Thermo Fisher Scientific, Czechia) with Schottky field emission gun (FEG). The micrographs of each sample were recorded in a series of nominal magnification in a backscattered electrons (BSE) and secondary electron detection regimes. In case of T-FD45 sample, energy-dispersive X-ray spectroscopy (EDS) was performed using Ultim Max detector (Oxford Instruments, UK) for elemental mapping of a single particle. The SEM micrographs were also used for image analysis.

4.1.2.3 Image analysis

The image analysis was performed with ImageJ v.1.53k software (National Health Institute, USA). Three SEM images of free surfaces for each powder at nominal magnification of 100× (∼150 particles per image) were used for determining the percentage of non-spheroidized particles and five images at nominal magnification of 300× (∼20 particles per image) for evaluation of particles' sphericity. The images were binarized using manual thresholding. Afterwards, a sequence of erosions, dilatations, and "fill holes" morphological operations was applied to separate individual particles and compensate polishing artefacts. The erosion erodes away the pixels on the edge of an object, while dilatation enlarges the object. Then, the particles in the micrographs were analysed, excluding particles on the photo edges and features below 25 μm^2 to eliminate noise and fine worn down particles. Clusters or sharp-edged particles were also excluded from sphericity evaluation. An example of image processing for circularity evaluation is shown in Figure 12. In the results, the term "circularity" will be used instead of "sphericity" as it is more appropriate when determining this information from two-dimensional images. To determine the percentage of particles unaffected by plasma jet, the "watershed" function was used in addition to the sequence of erosions, dilatations and "fill holes" operations to split the overlapping particles (Figure 12). Circular particles were counted automatically by the software, while the unprocessed particles were counted manually.

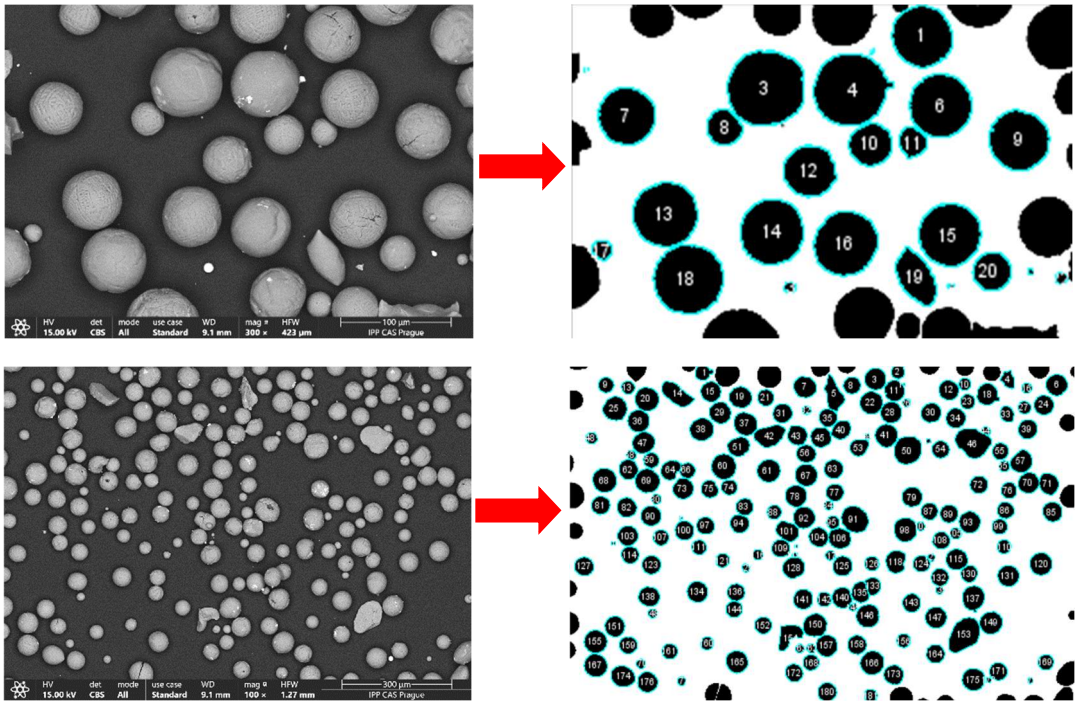

Figure 12: Image processing of circularity (upper couple) and evaluation of non-spheroidized particles (bottom couple). Original image (on the left) and binarized image with overlay and counted particles (on the right). Please note that particles leaning over micrograph edges were neglected.

4.1.2.4 Particle size analysis

The particle size distribution was measured using laser particle size analyser Mastersizer 3000 (Malvern, UK) equipped with a wet cell. The measured powder was poured into the cell filled with demineralized water until the analyser software showed sufficient detector saturation. After three measurements of powder, the in-built ultrasound in the cell was run for 30 s and the powder was remeasured three times. The purpose of ultrasound was to dissociate possible merged and agglomerated particles. Such conglomerations of particles could affect the particle size distribution towards higher particle sizes.

4.1.2.5 Flowability

The flowability was measured according to ASTM B213 standard, using Hall flow meter with two funnels of different outlet orifice sizes, 2.5 mm, and 5 mm, to compare the flowability through different sized orifices. For each measurement, 50 g of powder was poured into a funnel with the outlet orifice blocked by a dry and clean finger. Upon releasing the finger, the stopwatch was started and time elapsed for funnel emptying was recorded. Three measurements with each funnel were taken to obtain the average values. The powder apparent density was calculated from the weight of 25 cm^3 of the powders.

4.1.2.6 Chemical and phase composition

The evaluation of chemical and phase composition was carried out using XRD and XRF. The X-ray powder diffraction was performed with diffractometer D8 Discover (Bruker, Germany) with 1D detector LynxEye. The acquired diffraction patterns were evaluated using Rietveld refinement method for quantitative and qualitative phase composition of the powders. For the energy-dispersive X-ray Fluorescence, spectrometer S2 PUMA (Bruker, Germany) equipped with HighSense LE SDD detector was used.

4.2 Results

4.2.1 Task 1 – Designing the collecting chamber and spraying parameters

The first spheroidization experiment was carried out with the clay shale powder into the D1 chamber (Figure 13). It was observed already during the spraying that the powder was leaking through the cooling holes and through the inlet and rear opening. In addition, as plasma gases meet the partition, they are turned back and the already sedimented powder is stirred. The stream of gas driven by a plasma then escapes from the chamber and drags the stirred particles out of the chamber. As a result, only small amount of the powder was successfully collected, resulting in collection efficiency of only about 40 %. Besides the low collection efficiency itself, it was not possible to tell whether a certain amount of powder was, for example, evaporated or not, and, therefore, real effectivity of spheroidization using plasma torch assuming collecting all the spheroidized powder cannot be determined.

Figure 13: Clay shale powder before (left) and after (right) the spraying experiment.

For the D2 experiments, the lids were added to the front and rear ends to mitigate the particle loss through the wide openings of D1 chamber. Initially, the spraying distance of 250 mm was tried with the Al_2O_3 powder (A-SD250), but it was observed that with such long spraying distance, a lot of particles were rebounding from the front cover of the collector. Therefore, the spraying distance was shortened, to 150 mm (A-SD150a). However, the particles tended to form a coating on the partition in the chamber at the shorter spraying distance more easily, resulting in less collected powder. Moreover, the shorter spraying distance led to stronger particle flows swirling in the collector and thus to higher number of escaping particles.

The amount of powder collected in the D2 chamber in A-SD150a experiment was around 40 % of the powder fed in the plasma, i.e., similar ratio as with the D1 design. On top of that, additional approximately 10 % of the processed Al_2O_3 created the coating on the partition plate (Figure 14). Therefore, 60 % of the fed material was collected in total in the chamber, but on the expense of creating a thick deposit on the partition plate.

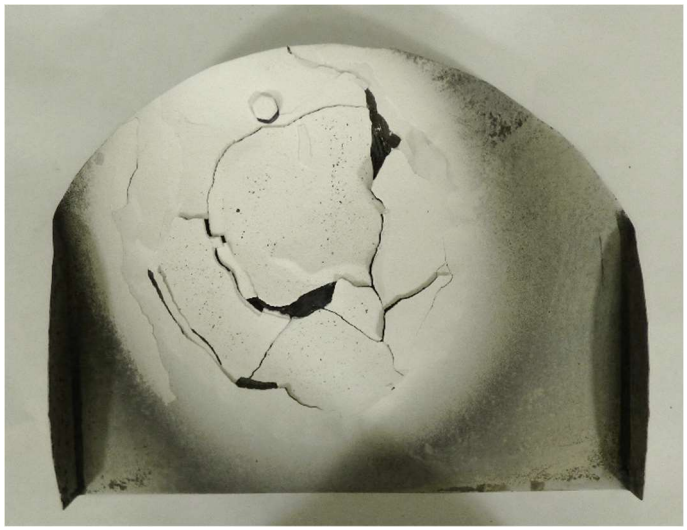

Figure 14: Al_2O_3 coating created on the partition plate.

In order to minimize the deposit formation, the partition was moved towards the rear end of the chamber, i.e., further away from the torch and from the particles' injection point (design D3). As a result, the total collection effectivity in case of A-SD150b experiment increased up to 70 % and the created deposit on the partition was thinner.

For design D4, the partition was moved to the position as in D2, but it was tilted towards the rear end of the vessel to create a shallower impact angle for the incoming particles. This way, the formation of the deposit was further suppressed and 93 % of fed material was captured, out of which 66 % was the powder and 27 % was the coating on the partition. Therefore, only 7 % of Al_2O_3 evaporated or escaped from the chamber through the chimney and the chamber inlet.

Table 3: Deposition efficiency of the chamber designs.

Design	Powder collected (%)	Deposit on partition
D1 (SD350)	~40	-
D2 (SD250)	~40	~10
D2 (SD150)	~40	~40
D3 (SD150)	~56	~10
D4 (SD150)	~66	~27

In conclusion, the D4 design was the most successful in terms of powder collection, accomplishing the purpose of collection efficiency more than 90 %, despite the formation of the deposit on the partition. Therefore, this collection chamber was used for further case studies on spheroidization of Al_2O_3 and TiC in the following section.

4.2.2 Task 2 – Spheroidization experiments – Al_2O_3

After setting up the collector design, more extensive experiments could be carried out. Al_2O_3 was sprayed in two experiments in order to evaluate the change in circularity, flowability, apparent density, particle size distribution and chemical and phase composition after the spheroidization. The difference in these properties between the angular feedstock powder, the powder spheroidized once and the powder spheroidized twice was observed.

4.2.2.1 Macroscopic and microscopic observation

After spraying, both A-SD150c and A2x-SD150 Al_2O_3 powders exhibited white colour like the starting feedstock powder (Figure 15). The powders gathered in the chamber in two preferential locations: one behind the frontal lid and second near the rear side lid. Therefore, these "heaps" of powder were collected separately in order to assess possible difference in powder properties.

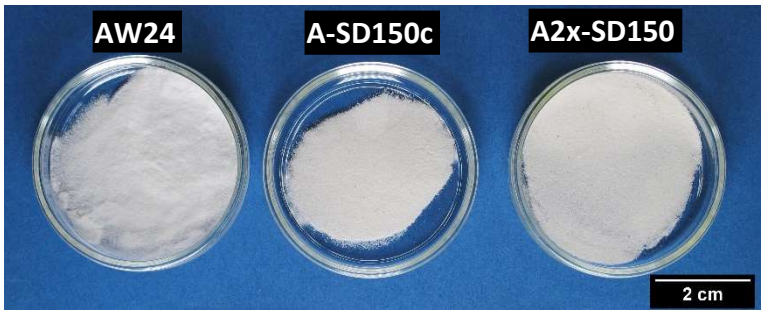

Figure 15: Al_2O_3 powder before and after the spraying experiment.

The cross-sections of the angular AW24 feedstock powder as well as the processed powders can be seen in Figure 16. In the micrograph of the AW24 powder, the sharp-edged and mostly elongated particles can be seen, which reflects their production by crushing. In micrographs of A-SD150c powder, mostly spheroidized particles can be observed. However, approximately 10 % of the particles were not spheroidized. These either had partly rounded corners, or were entirely angular as in the original feedstock, indicating insufficient contact with the hot plasma. In case of A2x-SD150 powder, the particles of which were exposed to the plasma twice, the amount of non-spheroidized particles was negligible. Any significant difference in the number of non-spheroidized particles between the powders collected in the front and the rear parts of the chamber were not observed.

Both, hollow and dense particles can be observed in micrographs of the samples A-SD150c and A2x-SD150 (Figure 16). The hollow particles contained either large central spherical cavities, or clusters of smaller pores scattered within the particles' volume. Moreover, some cavities have bright surface with visible dendritic structure of the particle, while some are dark or crumbled structure can be seen. Such dark cavities are

probably filled with epoxy resin that penetrated through the open cracks into the particle or crumbled during the grinding procedure.

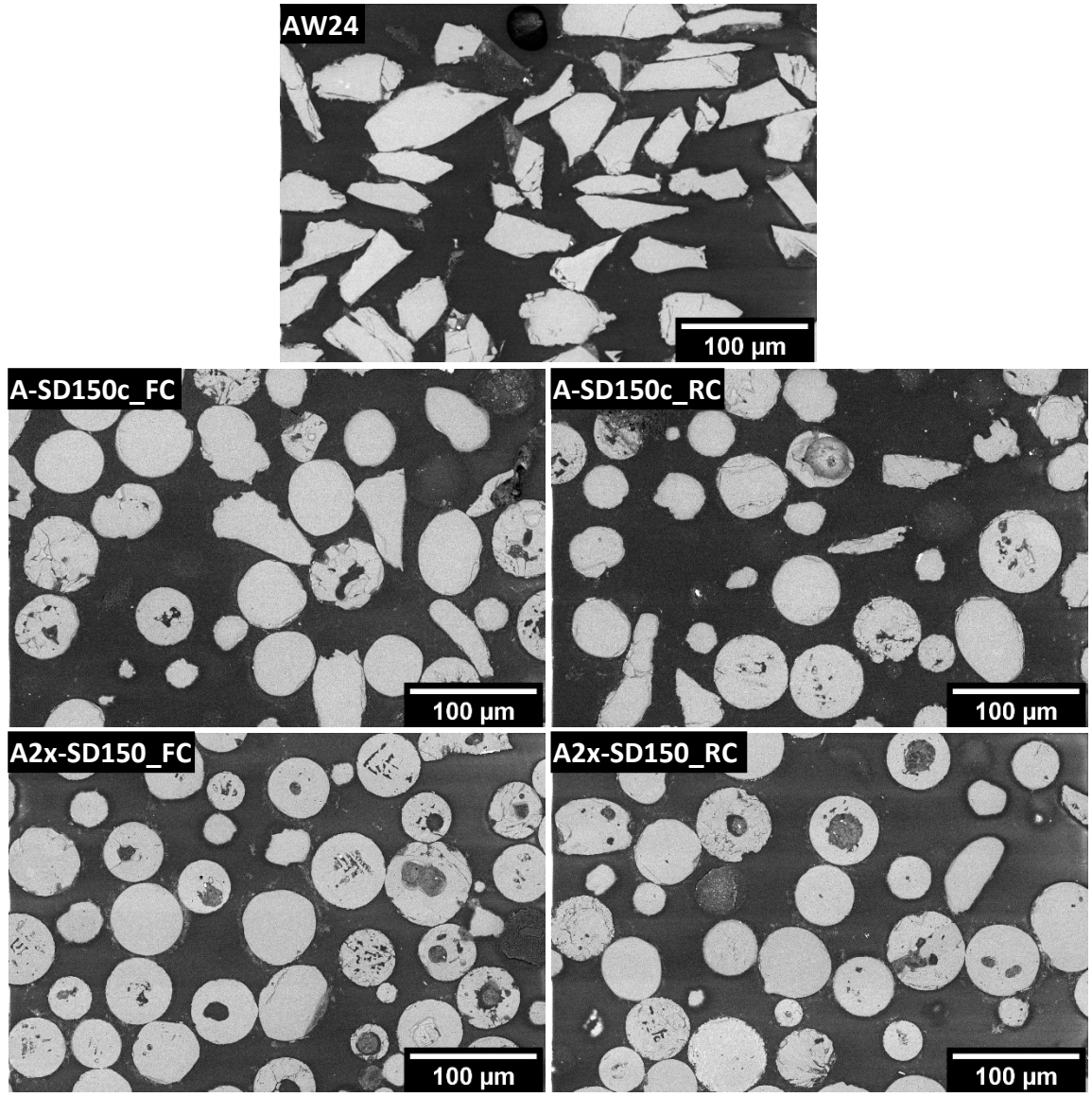

Figure 16: SEM micrographs of cross-sections of powders in BSE mode.

The SEM micrographs of free surfaces of AW24 powder and spheroidized powders are shown in Figure 17. Apart from the degree of spheroidization of the particles, the external structure of the particles can be seen. The AW24 feedstock powder exhibited characteristic cleavage fractures as a result of crushing of the brittle material during the manufacturing process. On the contrary, the spheroidized particles displayed either smooth surface, or dendritic structure on their surfaces. It can be assumed that the slower the cooling of a particle, the more developed dendritic structure. Furthermore, on the surface of some particles the cracks can be observed, presumably stemming from the particles' contraction during solidification. On both samples, brighter spots can be seen, being more frequent on A-SD150c particles than on A2x-SD150 particles. Using EDS, it was

confirmed that they were residuals of ZrO_2 powder sprayed in the experiments immediately before the spheroidization experiments.

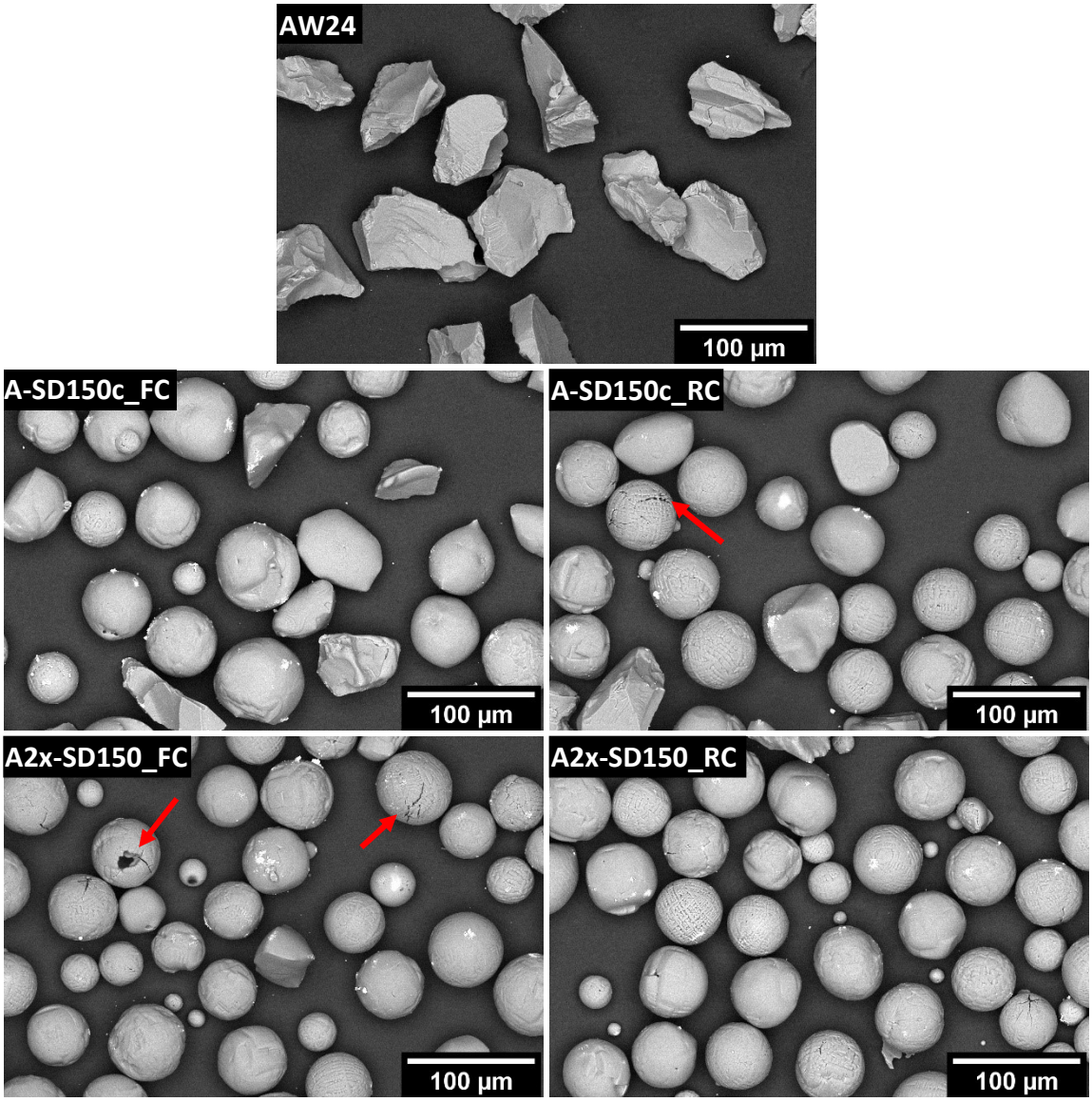

Figure 17: SEM micrographs of free surfaces of powders in BSE mode. The arrows mark the cracks in the particles.

In Figure 18, the detailed SEM micrographs of the spheroidized powders are shown. In the image of the A-SD250 sample, a cross-sectioned particle with a large cavity with a relief is shown together with a denser particle with small adjacent cavities. The image of A-SD150c_RC powder in SE mode shows two spherical particles with dendritic structures visible on their surface. Moreover, a crack can be seen in the smaller particle.

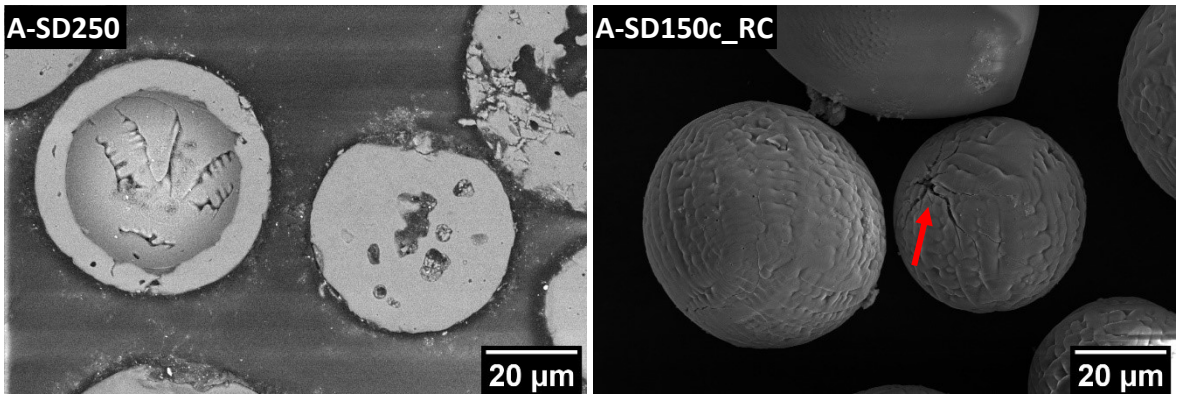

Figure 18: Detailed SEM micrographs of spheroidized particles. Left – cross-sections of particles, right – free surfaces of particles. The arrow mark the crack in the particle.

4.2.2.2 Image analysis

Ensemble results of the image analysis of the powders is shown in Figure 19. The amount of particles unaffected by the plasma jet in each sample is graphically represented together with the values of mean circularity. The highest percentage of unaffected particles, 10.34 %, was determined in the A-SD150c_FC sample, followed by 3.08 % in the A-SD150c_RC sample. While the amount of untreated particles is quite high in A-SD150c sample, negligible amount of such particles was determined in the A2x-SD150 sample. Similarly to the A-SD150c sample, in case of A2x-SD150 sample, slightly more unaffected particles were present in the front part of the chamber than in the rear.

The determined mean circularity values are graphically represented in Figure 19. The values confirmed the successful spheroidization as the mean circularity increased while the circularity scatter decreased after exposing the powders to the plasma jet. Moreover, the mean circularity further increased when the powder was exposed to the plasma for the second time (A2x-SD150 sample), effectively eliminating the unprocessed particles present in the powder after the first pass (A-SD150c sample).

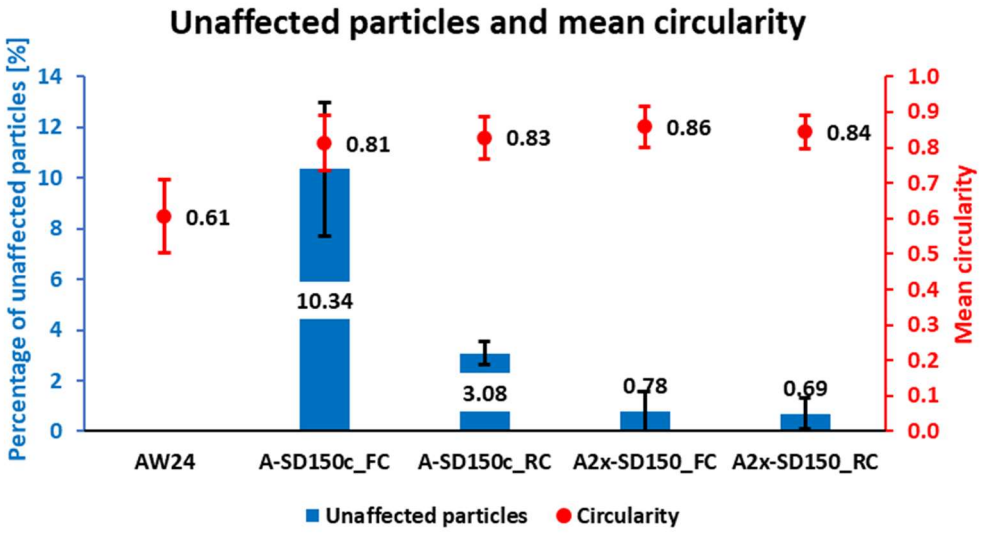

Figure 19: Percentage of particles unaffected by plasma jet and mean circularity values of the samples.

More detailed information about the mean sphericity of the particles can be obtained from the circularity distributions for each powder. The distributions are shown in Figure 20 for AW24 and A-SD150c powders and in Figure 21 for the A2x-SD150 powder. The shift of the peak of AW 24 powder in Figure 20 when compared to the peak of A-SD150c processed powder from 0.64 to 0.84 is evident. Further minor shift from 0.84 for A-SD150c powder in Figure 20 to 0.88 for A2x-SD150 powder in Figure 21 after the second spheroidization was observed, confirming the successful improvement of particles' sphericity by the repeated spheroidization of the powder. Only small percentage of particles exhibit the circularity higher than 0.92. This could be caused by the thresholding of analysed images as the brightness varies along the particles' edges, resulting in single pixels affecting the circularity determination.

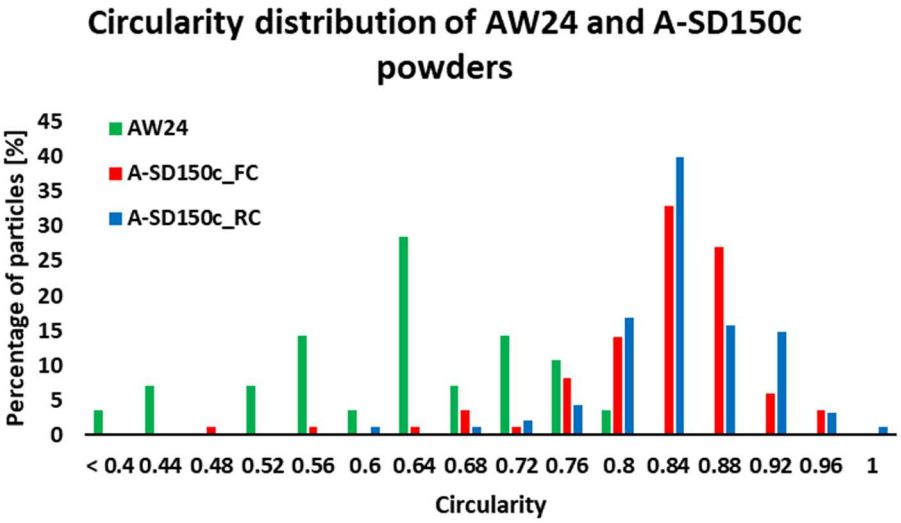

Figure 20: Circularity distribution of AW24 and A-SD150c powders.

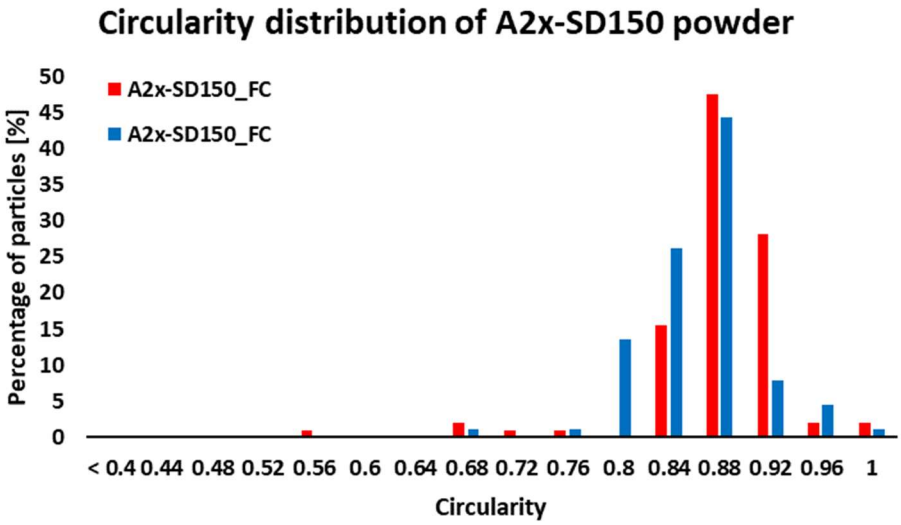

Figure 21: Circularity distribution of A2x-SD150 powder.

4.2.2.3 Particle size

In Table 4, the measured percentiles of particle size distributions are listed. The values for A-SD150c and A2x-SD150 powders show a significant decrease in Dv (50) and Dv (90) values and slight decrease in Dv (10) values when compared to the AW24 powder. Therefore, the size distribution of the sprayed powders became narrower when compared to AW24 powder. The effect of repeated spheroidization process on particle size was virtually negligible, demonstrating that Al_2O_3 undergoes during plasma treatment a very limited (if any) evaporation. The effect of 30 seconds ultrasound treatment of the samples was also negligible which demonstrated absence of loosely bound fine particles in the powder. The graphical representation of measured particle size distributions is shown in Figure 22.

Table 4: Particle size distributions.

[µm]	AW24		A-SD150C_FC		A-SD150C_RC		A2X-SD150_FC		A2X-SD150_RC	
	No US	US	No US	US	No US	US	No US	US	No US	US
Dv (10)	49.3	-	43.9	43.9	43.5	43.8	41.6	41.8	42.7	42.8
Dv (50)	72.3	-	58.8	58.1	57.6	57.5	55.4	55.7	57.5	57.3
Dv (90)	106	-	79.2	76.8	75.8	75.3	73.8	74	76.8	76.3

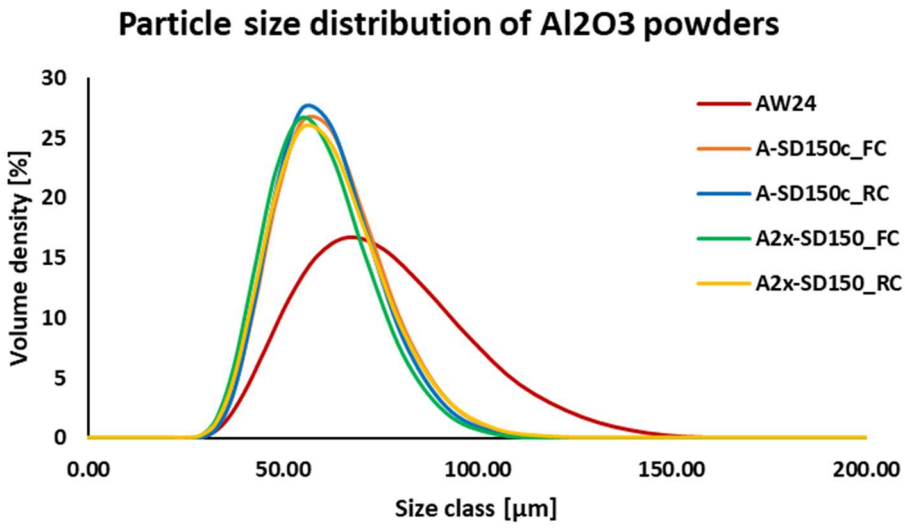

Figure 22: Particle size distribution curves of the Al_2O_3 powders.

4.2.2.4 Flowability and density

The flowability values for the powders using both 2.5 mm and 5 mm funnels are graphically represented in Figure 23. The AW24 powder is not included, because flowability of this powder was immeasurable with Hall flowmeter as the powder got stuck in both the funnels and could not flow through the orifice. After gentle tapping on the edge of the funnel (as recommended by ASTM B213 standard), only a small amount of powder passed through the orifice and a “rathole” in the powder in the funnel created. A batch of the AW24 powder was also dried in oven at 120 °C in attempt to dispose of possible moisture present in the powder possibly affecting the flowability. However, the dried AW24 powder did not flow through the funnels either. The flowability of the repeatedly spheroidized powder, A2x-SD150, increased slightly with respect to the A-SD150c powders and the increasing trend was confirmed by both funnel sizes. The influence of place of collection of the powder in the chamber on trend of flowability was not observed.

The apparent density values are listed in Table 5. The apparent density of the spheroidized powders increased when compared to the apparent density of AW24 powder which is in agreement with the idea of higher friction between the sharp-edged particles leading to their interlocking and eventually weaker ability to fill the voids

between the particles. The difference between the A-SD150c and A2x-SD150 powders was again negligible.

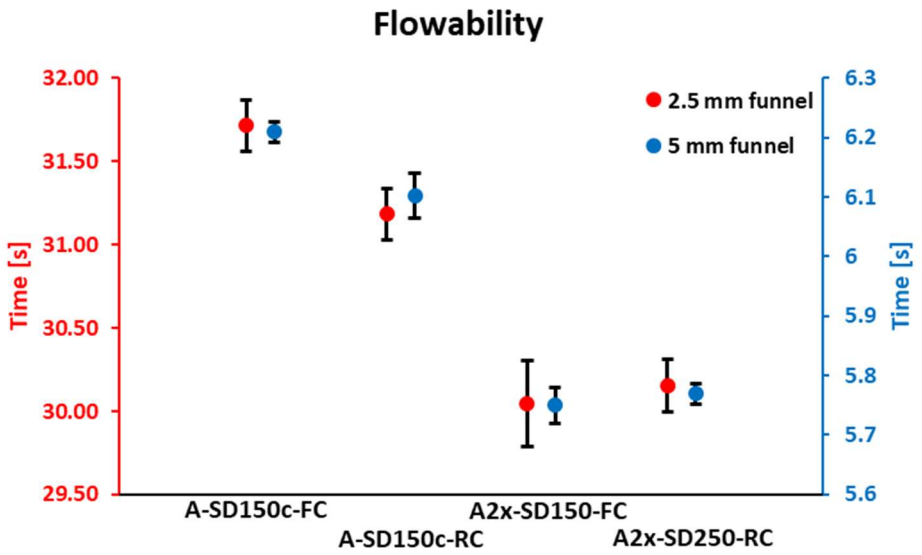

Figure 23: Flowability of the samples using two different funnels in Hall flowmeter.

Table 5: Apparent density of the powders.

	AW24	A-SD150c_ FC	A-SD150c_ RC	A2x-SD150_ FC	A2x-SD150_ RC
Apparent density [g/cm^3]	1.79 ± 0.02	2.00*	2.02*	2.02 ± 0.01	2.02*

* Only one measurement due to small amount of powder available.

4.2.2.5 Chemical and phase composition

The XRF chemical composition measurement showed the presence of more than 99 % of aluminium and negligible trace of other elements, of which zirconium was the most frequent in A-SD150c and A2x-SD150 samples, confirming the hypothesis of the contamination of the powder in the feeding lines (Table 6). The results of XRD measurements are listed in Table 7. The AW24 feedstock powder was pure α-phase Al_2O_3 (corundum). This phase was predominant also after the spheroidization experiments. However, phase transformations of corundum into the θ-phase and relatively rare δ-phase Al_2O_3 occurred. During the repeated spheroidization experiment with already spheroidized feedstock, the α-phase was prevalent again, but additional θ-phase and δ-phase-containing particles were formed. Also, the differences between powders collected from the front and the rear sections of the vessel were negligible.

Table 6: XRF measurement of the powders.

[%]	AW24	A-SD150c_FC	A-SD150c_RC	A2x-SD150_FC	A2x-SD150_RC
Al	99.73	99.35	98.97	99.15	98.89
Cl	0.21	0.23	0.25	0.24	0.23
Ca	0.06				
Fe			0.06	0.12	0.12
Zn				0.07	0.15
Y			0.06		0.04
Zr		0.41	0.66	0.42	0.55

Table 7: Phase compositions of the powders.

[%]	AW24	A-SD150C_ FC	A-SD150C_ RC	A2X-SD150_ FC	A2X-SD150_ RC
α-phase Al_2O_3	100	83.77	82.62	75.5	75.76
θ-phase Al_2O_3	0	11.85	12.51	16.29	17.54
δ-phase Al_2O_3	0	4.38	4.87	8.22	6.70

4.2.3 Task 2 – Spheroidization experiments – TiC

After the successful spheroidization experiments with Al_2O_3 powder, the TiC powder was attempted to spheroidize. Two different feeding distances were used in these experiments and the influence on the powders' properties was observed.

4.2.3.1 Macroscopical and microscopical observation

The TiC powder underwent a significant change during the spraying experiments. The TiC feedstock powder was deeply black, while the powders collected after the spraying were yellow-green (T-FD45 sample) and yellow (T-FD120 sample). Moreover, the processed material covered entirely inner surfaces of the collecting chamber, including the chimney (i.e., not only in the line of sight direction) and no preferential pile-up areas were observed. Therefore, all powder was collected together into one sample. When the experiment was repeated with longer feeding distance (T-FD120), the powder was yellow without any green tint (Figure 24).

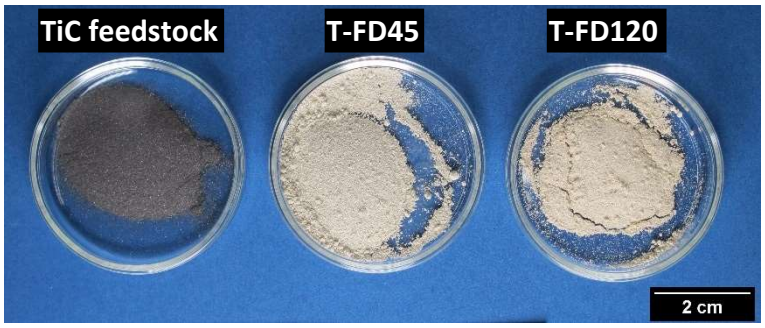

Figure 24: Powders before and after the TiC spraying experiment.

The SEM micrographs of the cross-sections of the sprayed powders are shown in Figure 25 (T-FD45 powder) and in Figure 26 (T-FD120 powder). Broad range of particle sizes can be observed in both T-FD45 and T-FD120 samples from tens of micrometres to even nano-sized particles. The particles of both powders were mostly spherical. In T-FD45 sample, two-phase particles were observed in BSE mode sensitive to local mean atomic number (Figure 25). Brighter phase often created a core of the particle covered in a shell of a darker phase. In the second experiment (T-FD120), the two-phase particles were no longer present in the sample (Figure 26).

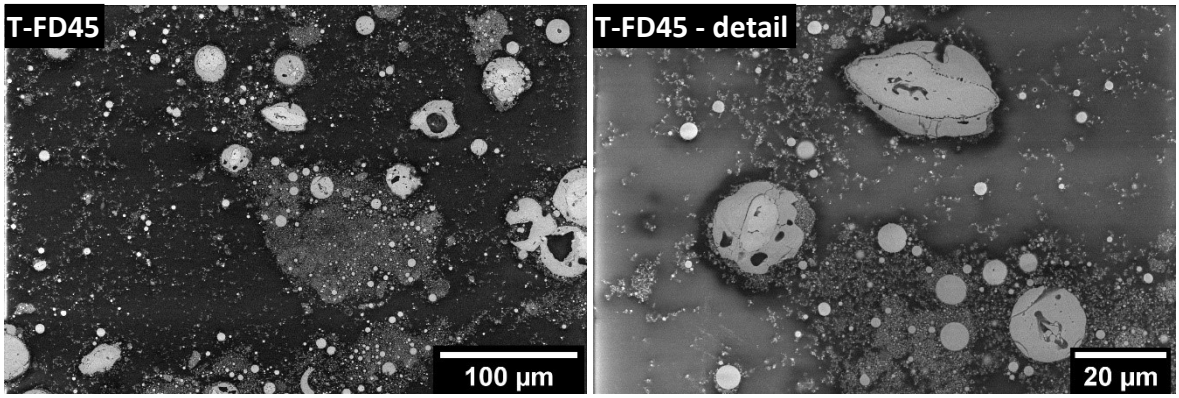

Figure 25: SEM micrographs of cross-section of T-FD45 powder.

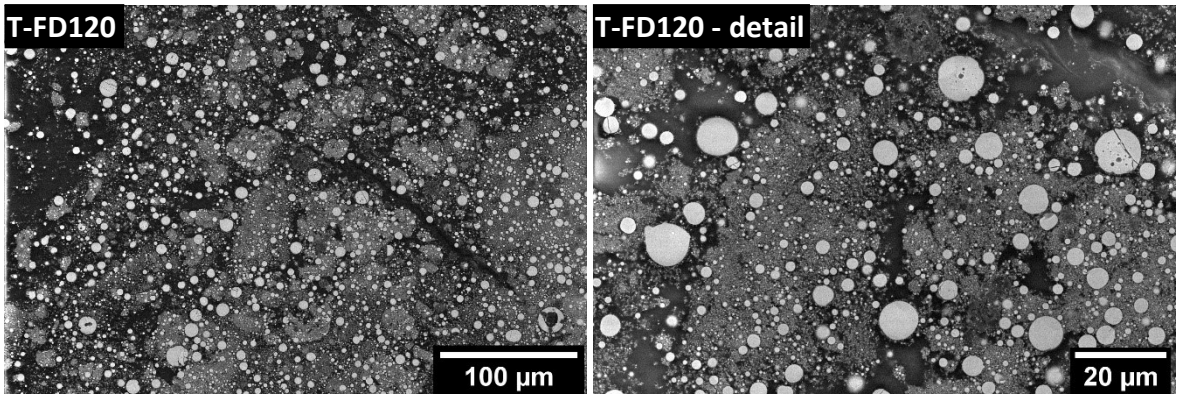

Figure 26: SEM micrographs of cross-section of T-FD120 powder.

The SEM micrographs of free surfaces of TiC feedstock powder are shown in Figure 27, followed by the free surfaces of T-FD45 and T-FD120 samples in Figure 28 and Figure 29 respectively. In the detailed Figure 27, it can be seen that, similarly to the T-FD45 and T-FD120 samples, the particle size distribution of the TiC feedstock powder was also wide. According to Figures 28 and 29, the spherical particles were achieved in both experiments. The two-phase composition of the T-FD45 powder is not visible on free surfaces micrographs, which corresponds to the core-shell type of particle morphology, which was visible on the cross-sections. In detailed micrographs in Figure 29, very fine particles adhering to the larger ones can be observed. Details of these nanosized particles are shown in Figure 30.

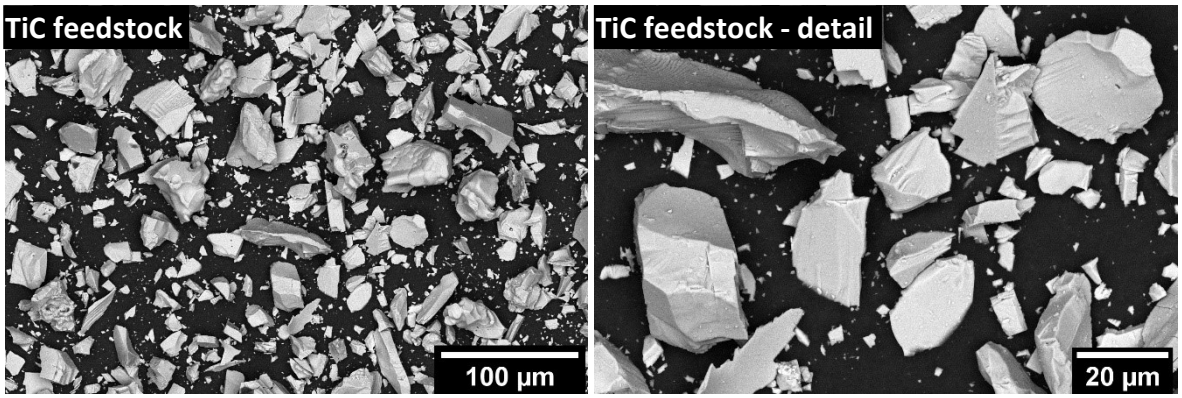

Figure 27: SEM micrographs of TiC feedstock powder.

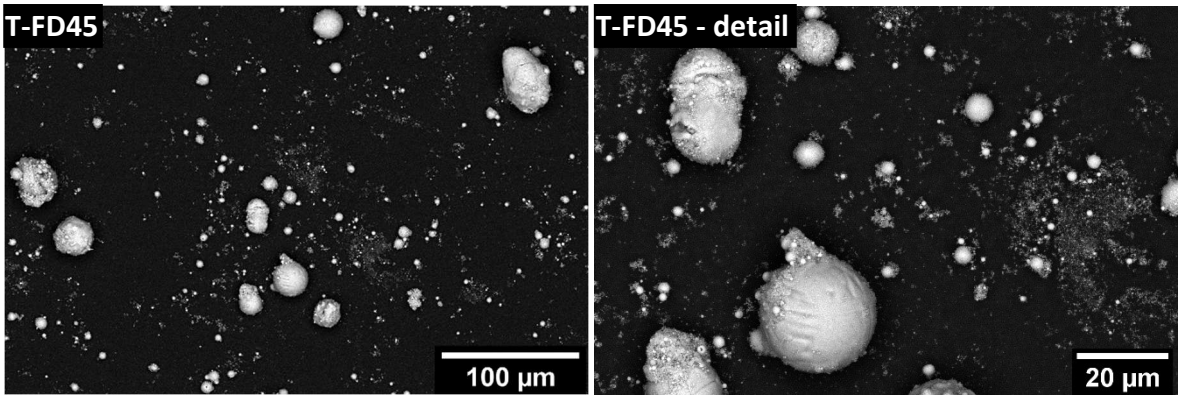

Figure 28: SEM micrographs of free surface of T-FD45 powder.

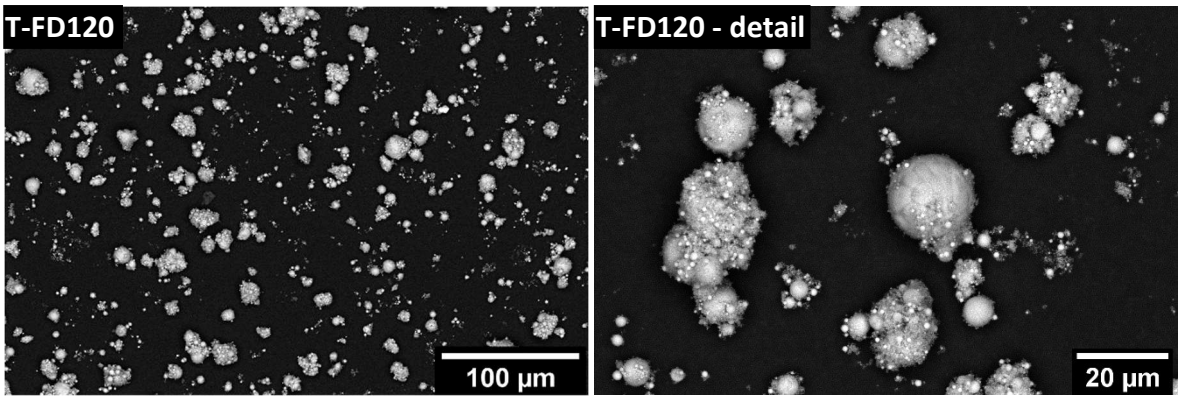

Figure 29: SEM micrographs of free surface of T-FD120 powder.

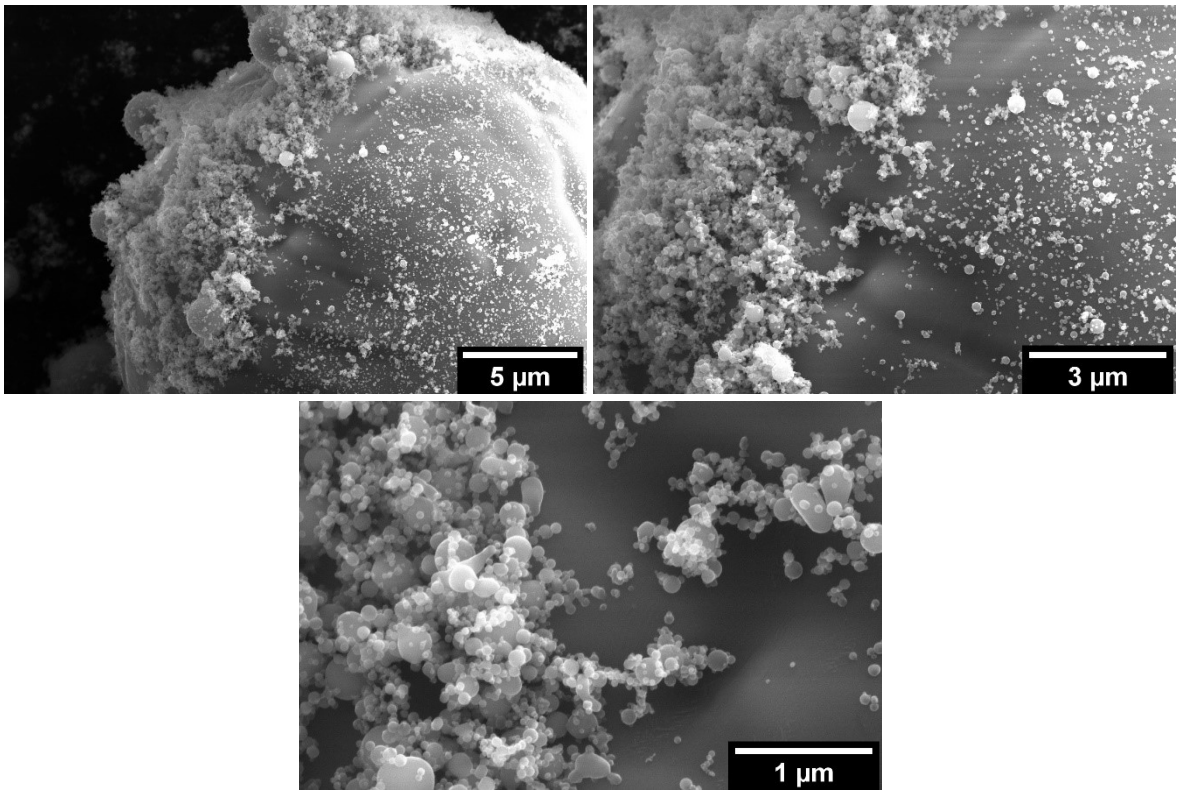

Figure 30: Detail surface of particle from Figure 28 (T-FD45 sample) in high resolution and SE imaging mode.

In order to observe the composition of two-phase particles of the T-FD45 sample, EDS mapping was performed. The qualitative maps showing the different content of titanium, carbon, and oxygen in different spots of the particles are shown in Figure 31. The results show increased content of titanium in the core of the particles. The carbon is present in most of the mapped area due to its abundance in epoxy resin. However, higher amount of carbon is present in the cores of the particles when compared to their shells. On the contrary, higher amount of oxygen is present in the shells in comparison with the cores.

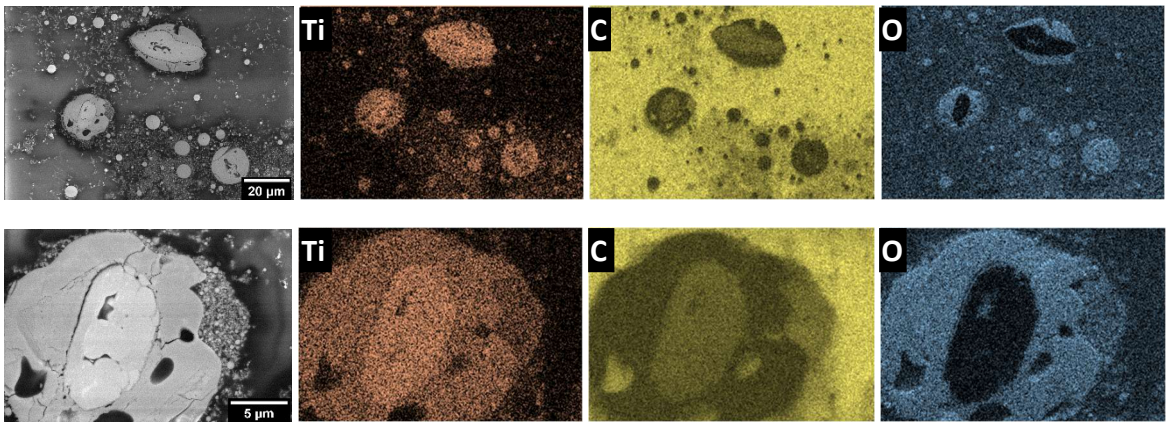

Figure 31: EDS mapping of T-FD45 powder particles.

An EDS line scan was performed showing the profile of titanium, carbon, and oxygen across the shelled particle (see Figure 32). It can be seen in Figure 32 that the amount of titanium and carbon increases in the core of the particle, while the oxygen amount decreases. Small amount of silicon was also detected with the line scan, which comes mostly from the grinding and polishing residues from the metallographic preparation trapped in the pore. It may be concluded that the two-phase particles consisted of original TiC (core) covered by newly formed TiO_2 (shell).

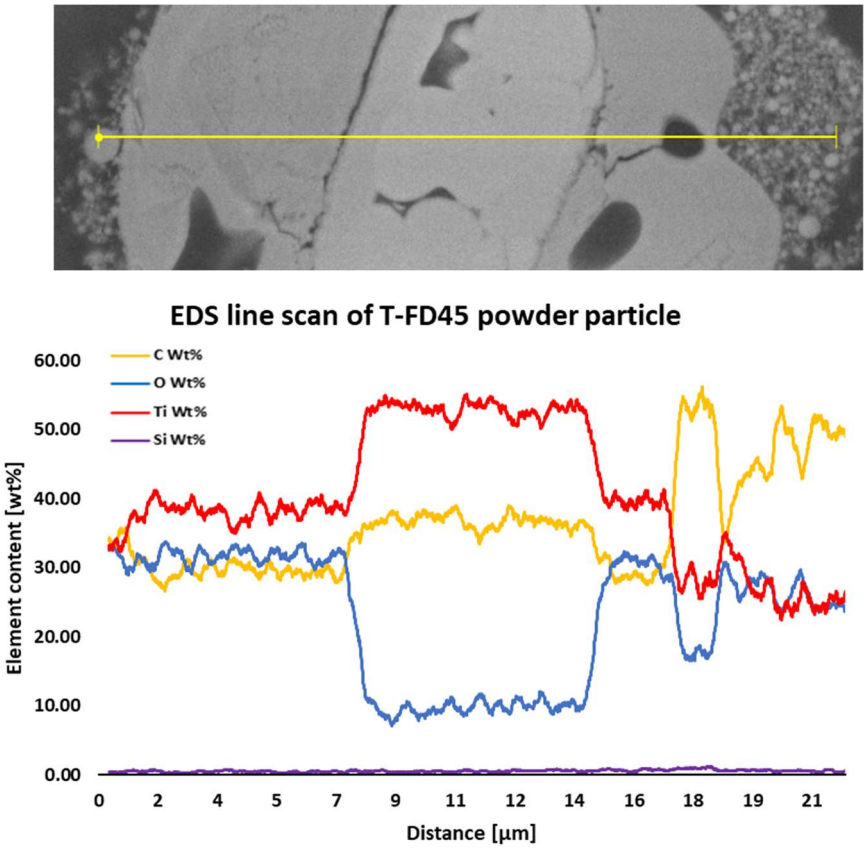

Figure 32: Line scan of the two-phase particle in the T-FD45 sample. The curves show moving average with period of 35 points of the measured data.

4.2.3.2 Particle size

The particle size distributions as observed by particle size analyser are listed in Table 8 and graphically represented in Figure 33. Unlike the Al_2O_3 powder, the 30 seconds of ultrasound treatment of particles made a notable difference in particle size distribution in case of T-FD45 and T-FD120 powders. Therefore, it can be assumed that after the spraying, the particles were merged into the clusters which were broken apart by the ultrasound treatment. All the values, Dv (10), Dv (50), and Dv (90) decreased significantly after the spraying when compared to the feedstock TiC powder, resulting in very fine powders with most of the particles smaller than 10 µm. On the contrary, the feeding distance did not affect the size of particles significantly. In Figure 34, trimodal particle size

distribution was observed for the spheroidized powders, as compared to unimodal distribution of the feedstock.

Table 8: Particle size distributions.

[µm]	TiC		T-FD45		T-FD120	
	No US	US	No US	US	No US	US
Dv (10)	10.5	9.0	2.3	0.5	1.7	0.4
Dv (50)	29.2	28.3	19.6	4.5	12.0	6.0
Dv (90)	57.0	57.4	55.2	13.1	31.9	11.2

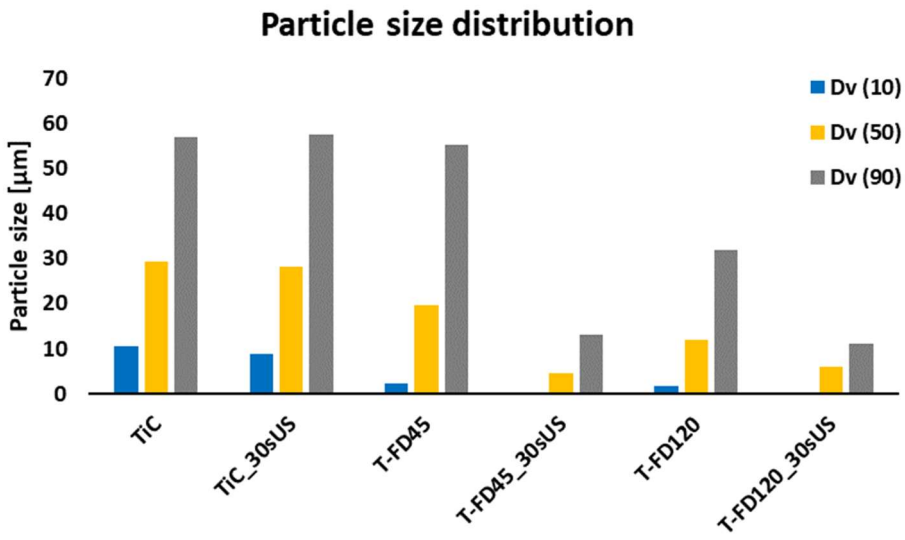

Figure 33: Particle size distributions.

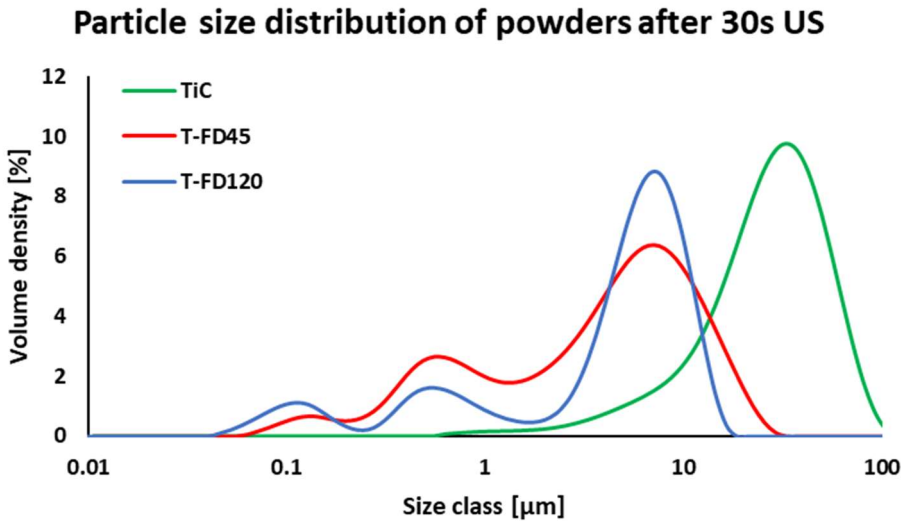

Figure 34: Particle size distribution curves of the samples after the ultrasound treatment.

4.2.3.3 Flowability and apparent density

The flowability of the TiC feedstock powder as well as that of the T-FD45 and T-FD120 powders was immeasurable with Hall flowmeter. The powders entirely clogged the orifice, so that even tapping on the funnel did not make the powder flow through. The determined apparent density values are listed in Table 9. In case of the TiC feedstock powder, the apparent density was 1.57 g/cm^3. The apparent density of T-FD45 and T-FD120 processed powders was comparable and dropped to about 30 % of the original feedstock density.

Table 9: Apparent density of the powders.

	TiC	T-FD45	T-FD120
Density [g/cm^3]	1.57 ± 0.01	0.56 ± 0.07	0.55 ± 0.02

4.2.3.4 Chemical and phase composition

The XRF measurement was not able to evaluate the carbon content, but both T-FD45 and T-FD120 powders showed presence of nearly 99 % of titanium accompanied with small amounts of aluminium, silicon, vanadium, and iron (Table 10). The XRF measurement of TiC feedstock powder was not performed. The XRD results are listed in Table 11 and graphically represented in Figure 35. Both sprayed powders contained mostly TiO_2 in its polymorphs rutile and anatase in comparable amounts. Only 3.79 % of TiC was detected in the T-FD45 powder and none was detected in T-FD120 powder, which is in accordance with the SEM and EDS observation of core-shell particles in T-FD45 sample. A small amount, 2.37 %, of graphite was detected in original TiC powder.

Table 10: XRF measurement of the powders.

[µm]	T-FD45	T-FD120
Al	0.27	0.05
Si	0.20	0.21
Ti	98.76	98.91
V	0.31	0.33
Fe	0.38	0.41
Zr	0.04	0.04
Cl	0.04	0.04

Table 11: Phase composition of powders according to XRD measurement.

[µm]	TiC	T-FD45	T-FD120
TiC	97.63	3.79	0
Graphite	2.37	0	0
TiO_2 – Rutile	0	69.03	70.46
TiO_2 – Anatase	0	27.18	29.54

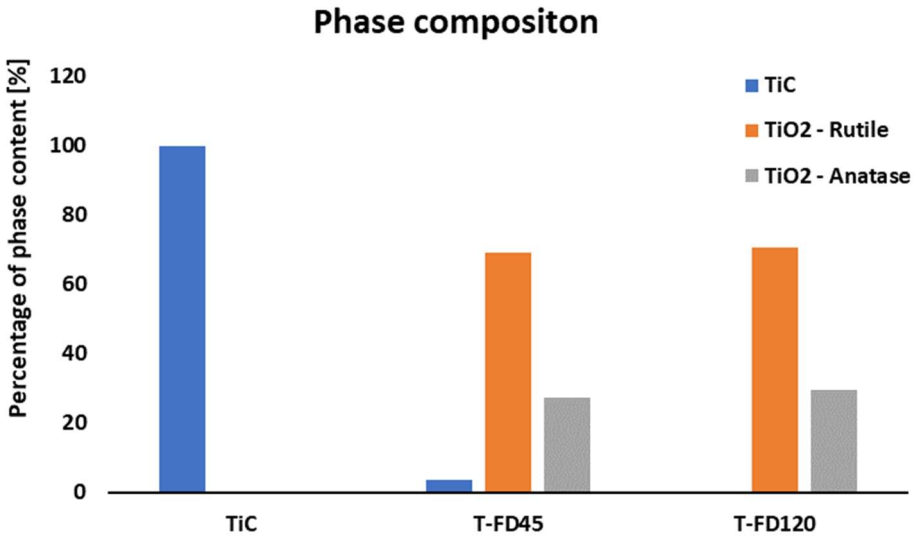

Figure 35: Phase composition of powders according to XRD measurement.

4.3 Discussion

4.3.1 Task 1 – Development of the collection chamber

The experimental part of this thesis was divided in two parts. The first part was focused on designing the experimental chamber for the purpose of collecting the powder spheroidized with use of plasma spraying. Five testing experiments with clay shale and Al_2O_3 powders were performed, between which the chamber was improved iteratively. The main goal of the improvements was to maximise the collecting efficiency. After the improvements, such as change cooling mechanism of the chamber, tilting the partition plate inside the chamber and sealing of the joints, the collection efficiency of 93 % was achieved. However, it should be admitted that part of the fed material was deposited onto the partition plate, thereby lowering the effective particle yield to 66 % of the injected powder. Nevertheless, this drawback of the collection chamber was caused by the limited space available in the spray shop. In a large-scale industrial application, this could be easily prevented by using, e.g., a longer collection vessel to allow in-flight cooling and gravitational settling of all the particles, thereby achieving higher powder yield.

4.3.2 Task 2 – Spheroidization experiments - Al_2O_3

The second part of the study was dedicated to spheroidization of Al_2O_3 and TiC powders using the plasma torch and the collecting chamber developed in the previous part. Two experiments were performed for each material.

For Al_2O_3, the first one was carried out using the final spraying parameters established during the development and testing of the chamber. For the second experiment, part of the powder spheroidized in the first experiment was used as the feedstock and spheroidized again using the same parameters. In both experiments, the sprayed powders were collected at two places in the chamber to assess potential differences in particle characteristics. The microscopic observation revealed successful spheroidization of powders. In the powder A-SD150c_FC collected in the front part of the chamber, more particles untreated by the plasma jet were observed when compared to the A-SD150c_RC powder collected in the rear part. This was further confirmed with the image analysis of the powders. Although the powders swirl a lot in the chamber during spraying, the most probable reason for this phenomenon is that these particles did not penetrate into the jet. Instead, they were driven by the flow of the plasma through the inlet hole, and they left the gas flow right after they entered the chamber. This indicates that the powder injection nozzles may require design optimization. When the spheroidization of the powder was repeated (the A2x-SD150 sample), the percentage of untreated particles decreased significantly to less than 1 % with the current setup. In other words, a repeated spheroidization of the powder is recommended in order to obtain more than 99 % of the spherical particles. In [8], Zhang et al. studied

spheroidization of yttria-stabilized zirconia powder using atmospheric plasma spraying and 95 % of spherical particles were achieved.

Even though many hollow particles were observed in the SEM, the majority of particles was dense, which should be presumably attributed to fact that the feedstock particles were already dense. Moreover, according to the SEM micrographs of particles' free surfaces, numerous particles had cracks on their surface. These may extend through the entire thickness of the shell and served as gas vents from the particle cores. As a result, the gas did not expand inside the particles to form a large cavity and smaller collapsed cavities were formed instead.

On the free surfaces of powders in SEM, especially on A-SD150c sample, small particles of zirconia were attached to the larger Al_2O_3 particles. Despite thorough cleaning of the vessel before spraying, these particles possibly originated from the previous spraying experiment with zirconia powder. This powder consisted of fine agglomerates which were easy to break, and they contaminated the feeding lines. Therefore, the proper cleaning of the current spheroidization facility, i.e., the collection chamber and the feeding systems, can be challenging and its design should be further upgraded in order to allow easier cleaning. On the other hand, minor contamination by ZrO_2 did not anyhow change the results obtained within this study.

The image analysis was also used to evaluate the sphericity (3D characteristic) of the particles which was represented by the circularity (2D projection) values as obtained from the micrographs. The results showed that the repeatedly spheroidized particles (A2x-SD150) were slightly more spherical than the particles spheroidized only once (A-SD150c). The relevant difference between the circularity of powders collected in the front and the rear part of the chamber was not observed. Only a small number of particles exhibited the circularity value higher than 0.9, which was probably caused by the image resolution, which is a common problem when evaluating circularity, as was reported in [39]. The boundary between the particles and their background was not created by a smooth line, which in turn affected the circularity evaluation. It can be also speculated, that the semi-molten particles could be also slightly elongated in the flight direction.

The results of particle size analysis showed the similar particle size distribution of A-SD150c and A2x-SD150 samples regardless of the number of spheroidization runs. The use of ultrasound treatment of the particles made no difference in the particle size distribution either, indicating no agglomeration of the collected powders. The size distribution of particles shifted towards lower values during the spheroidization when compared to the original AW24 feedstock powder. The larger measured size values of AW24 powder particles are probably given by the principle of measurement when the

longer diameter of elongated coarse particles is measured. Therefore, the volume of the particles was presumably unchanged.

The increased sphericity of the sprayed powders was also proven by measurement of powders' flowability. The flowability of the AW24 feedstock powder was immeasurable (i.e., poor flowability) and was significantly improved by the plasma treatment. Further slight improvement of flowability was achieved by a repeated spheroidization (A2x-SD150 sample), which is in accordance with the circularity values (compare Figure 19 and Figure 23), i.e., the higher the mean circularity, the higher the flowability. The area of collection of power did not significantly influence the flowability. Also, the apparent density of both the spheroidized powders collected at either place in the chamber were almost identical. Both spherical powders were denser than the angular AW24 feedstock powder showing higher packing density of the spherical particles when compared to the sharp edged irregular shaped particles.

Chemical composition evaluated using XRF confirmed nearly pure aluminium (oxide). Only small amount of zirconium was recorded, the presence of which was attributed to the insufficient cleaning of the collection facility prior to the experiments. The XRD measurement showed that the α-phase Al_2O_3 was predominant in the powders after the spraying, which is the intended result. Only relatively small percentages of metastable θ- and δ-Al_2O_3 phases were recorded. After the repeated spheroidization, further increase in presence of θ and δ-Al_2O_3 phases was observed.

In [48], atmospheric plasma spraying was successfully used to spheroidize barium titanate. Moreover, a plasma sprayed coating was then prepared from the spheroidized feedstock. The result showed that such coatings have improved dielectric properties and hardness. It was also reported, that when the feedstock powder contained voids, the additional pores were introduced into the coating structure. Therefore, further investigation of preparing the coatings from spheroidized hollow powders can follow up on this thesis.

4.3.3 Task 2 – Spheroidization experiments - TiC

The second part of Task 2 was dedicated to the spheroidization of TiC. The processed material was collected as a very fine deposit on the internal surfaces of the collection chamber, rather than as piles of settled powder on the container bottom. Moreover, unlike in the Al_2O_3 spheroidization experiment, no coating was formed on the partition in the chamber. The collected powder was yellowish in colour and the phase composition analysis revealed that the feedstock material oxidized into TiO_2, which was also confirmed by phase analysis using XRD. Consequently, the experiment was attempted with prolonged feeding distance in order to decrease the particles' dwell time in the plasma jet, resulting in decrease of the thermal input and the oxidation of the feedstock. Despite the modified feeding conditions, the sprayed powder was again in the

shades of yellow and the decomposition of the feedstock was again confirmed using XRD measurement of the powder and EDS on the powder cross-sections. This result is in accordance with literature [49] where oxidation kinetics of TiC in dry synthetic air was studied. It was observed that oxidation of TiC particles in air begins, depending on their size, at as low as 200 – 400 °C and is finished at 1000 – 1200 °C.

Using the SEM, spherical particles in broad range of particle sizes from nanometres up to tens of micrometres were observed in case of both, T-FD45 and T-FD120 powders. The nano-sized particles were observed to be adhering to the larger particles. In the T-FD45 sample, particles composed of TiC core and TiO_2 shell were present. These particles resulted from the incomplete transformation of TiC into TiO_2. In T-FD120 sample, these two-phase particles were not found, although the TiC particles spent shorter time in the plasma plume in this experiment. One of the probable explanations of this phenomenon might be that when the particle was introduced into the plasma at the lower feeding distance, where the temperature is higher, the TiO_2 shell formed rapidly, hindered further ingress of oxygen, and preserved the TiC core inside. When the temperature was lower, the TiC transformed slowly, but completely. Other explanation can be that the particles introduced into the plasma at lower feeding distance gain higher speed and, therefore, they leave the plasma more quickly so that the full transformation cannot proceed. A third possible scenario is the rebounding of several particles from the denser jet core when injected closer to the plasma nozzle (feeding distance of 45 mm). As a result, these particles left the hot part of the jet immediately and their transformation was not completed. On the contrary, the longer feeding distance possibly led to more efficient particle penetration into the less dense yet still hot plume of the plasma gases, enabling more thorough heating and transformation of all particles.

During the spraying experiments, the particle size changed significantly in case of both T-FD45 and T-FD120 powders. The most significant decrease was determined in case of the Dv (10) value. The decrease was not so obvious in case of measuring without ultrasound treatment, but when the treatment was performed, the clusters of particles adhering to each other were disintegrated and the representative particle size distribution was measured.

Flowability of the TiC feedstock and of the spheroidized powders was immeasurable using Hall flow meter due to the small particle size of the powders. The presence of fine particles in the size distribution increases the specific surface area, and thus, for example, moisture can be reportedly increased [38]. The apparent density of both spheroidized powders decreased significantly with respect to the feedstock powder due to its phase transformation (i.e., decrease in true density from 4.9 g/cm^3 of the TiC [50] to ~4.1 g/cm^3 of the mixture of the TiO_2 polymorphs [51]) as well as its reduced particle size.

The XRD measurement was used to confirm the microscopic observation and the EDS measurement. A small amount of TiC was reported in the T-FD45 sample, while none was reported in the T-FD120 sample. With XRD measurement, the transformation of TiC into TiO_2 was confirmed, dominantly as rutile and less as anatase. With the higher feeding distance, the transformation of TiC into TiO_2 was completed, unlike the spraying with lower feeding distance. Graphite present in the original feedstock may be expected to be fully oxidized into gaseous CO or CO_2.

5 Conclusions

In this thesis, the facility suitable for spheroidization of powders with WSP-H plasma torch was designed. The chamber employed in similar experiments in the past was used as a basis for the newly redesigned chamber. Several factors needed to be considered while designing the chamber, such as limited space for the chamber in the spraying laboratory, cooling of the chamber due to immerse heat generated by the torch, losing the powder due to its intense swirling or creation of a coating inside the chamber. The main goal was to maximise the collecting efficiency. The collecting efficiency of 93 % of material, of which 66 % was the spheroidized powder and 27 % was the coating on the partition inside the chamber, was achieved after several improvements of the collecting chamber and the spraying parameters.

The spheroidization experiments with Al_2O_3 and TiC powders were then performed employing the redesigned collection chamber. Two experiments with Al_2O_3 powder were performed, in which the AW24 powder was spheroidized and part of the spheroidized powder was used again as a feedstock for the second spheroidization experiment. It was shown that after the first spheroidization pass, about 90 % of the particles were spherical. The spheroidized powder exhibited significantly improved flowability and about 10 % increased apparent density. Phase composition of the feedstock was mostly preserved as only 16 % of the original α phase was transformed to θ and δ phases. The second spheroidization pass further increased the number of spherical particles to >99 %, slightly improved flowability and induced further α phase transformation to the metastable phases.

After the successful experiments with Al_2O_3 powder, another two experiments were performed with TiC powder, in which the influence of two different feeding distances was studied. The shorter feeding distance led to nearly complete transformation of TiC into TiO_2 with the formation of a limited number of two-phase particles, where the TiC core was encapsulated in TiO_2 shell. The prolonged feeding distance resulted in complete phase transformation of the carbide feedstock into the oxidic collected powder. Both processed powders were spheroidized, but neither of them was measurable using the Hall flow meter due to the very fine particle size distribution and particles agglomeration. The apparent density of the processed powders was lower than that of the starting feedstock by approximately 65 %.

References

[1] DAVIS, J. *Handbook of Thermal Spray Technology* [online]. Materials Park, OH, USA: ASM International : Davis, J.R. ed., 2004. ISBN 0-87170-795-0.

[2] PAWLOWSKI, L. *The Science and Engineering of Thermal Spray Coatings: Second Edition* [online]. B.m.: John Wiley and Sons, 2008. ISBN 9780471490494.

[3] PRESCOTT, J. K. and R. A. BARNUM. On powder flowability. *Pharmaceutical Technology*. 2000, **24**(10), 60-84+236. ISSN 01478087.

[4] BAO, Q., Y. YANG, X. WEN, L. GUO and Z. GUO. The preparation of spherical metal powders using the high-temperature remelting spheroidization technology. *Materials and Design* [online]. 2021, **199**. ISSN 18734197. doi:10.1016/J.MATDES.2020.109382

[5] KUMAR, S. and V. SELVARAJAN. Spheroidization of metal and ceramic powders in thermal plasma jet. *Computational Materials Science* [online]. 2006, **36**(4), 451–456. ISSN 0927-0256. doi:10.1016/J.COMMATSCI.2005.09.001

[6] Gulyaev, I. *Tailoring of powders for plasma production of hollow ceramic spheres* [online]. Conference Paper, International Symposium on Advanced Materials and Technologies, 2013.

[7] REED, J. S. *Principles of Ceramics* [Online]. Second Edition. John Wiley and Sons, New York, USA, 1995. ISBN 0-471-59721-X

[8] ZHANG, X., K. ZHOU, F. CHANG, Ch. SONG, Ch. DENG and S. LIANG. Yttria-stabilized-zirconia hollow spheres prepared by atmospheric plasma spray. *Particuology* [online]. 2014, **14**, 57–62. ISSN 1674-2001. doi:10.1016/J.PARTIC.2013.06.003

[9] ZENG, S., M. XIAO, X. LIU, Y. WU, K. LI, Z. QIU and D. ZENG. Effects of process parameters on morphologies of titanium carbide powder by thermal plasma treatment. *Mater. Res. Express* [online]. 2019, **6**, 1265–1270. doi:10.1088/2053-1591/ab5ddb

[10] CHATURVEDI, V., P. v. ANANTHAPADMANABHAN, Y. CHAKRAVARTHY, S. BHANDARI, N. TIWARI, A. PRAGATHEESWARAN and A. K. DAS. Thermal plasma spheroidization of aluminum oxide and characterization of the spheroidized alumina powder. *Ceramics International* [online]. 2014, **40**(6), 8273–8279. ISSN 0272-8842. doi:10.1016/J.CERAMINT.2014.01.026

[11] ESPIE, G., A. DENOIRJEAN, P. FAUCHAIS, J. C. LABBE, J. DUBSKY, O. SCHNEEWEISS and K. VOLENIK. In-flight oxidation of iron particles sprayed using gas and water stabilized plasma torch. *Surface and Coatings Technology* [online]. 2005, **195**(1), 17–28. ISSN 0257-8972. doi:10.1016/J.SURFCOAT.2004.05.030

[12] DUDIK, J. *Vliv přítomnosti miniaturních splatů na mechanické vlastnosti hybridních plazmových nástřiků*. Bachelor thesis. Prague: DM-FNSPE-CTU, 2020.

[13] DUDIK, J. *Multilevel evaluation of mechanical properties of hybrid plasma sprayed coatings.* Research assignment work. Prague: DM-FNSPE-CTU, 2021.

[14] HRABOVSKY, M., V. KOPECKÝ, V. SEMBER, T. KAVKA, O. CHUMAK and M. KONRAD. Properties of hybrid water/gas dc arc plasma torch. *IEEE Transactions on Plasma Science* [online]. 2006, **34**(4 III), 1566–1575. ISSN 00933813. doi:10.1109/TPS.2006.878365

[15] VOLENÍK, K., F. HANOUSEK, P. CHRÁSKA, J. ILAVSKÝ and K. NEUFUSS. In-flight oxidation of high-alloy steels during plasma spraying. *Materials Science and Engineering: A* [online]. 1999, **272**(1), 199–206. ISSN 0921-5093. doi:10.1016/S0921-5093(99)00478-5

[16] STUNDA-ZUJEVA, A., Z. IRBE and L. BERZINA-CIMDINA. Controlling the morphology of ceramic and composite powders obtained via spray drying – A review. *Ceramics International* [online]. 2017, **43**(15), 11543–11551. ISSN 02728842. doi:10.1016/J.CERAMINT.2017.05.023

[17] FOGLER, B. B. and R. v. KLEINSCHMIDT. Spray Drying. *Industrial and Engineering Chemistry* [online]. 2002, **30**(12), 1372–1384. ISSN 00197866. doi:10.1021/IE50348A007

[18] ANDERSON, I. E. and R. S. FIGLIOLA. Observations of gas atomization process dynamics. *Materials Science* [Online]. 1988, 205–223.

[19] XIA, Y. and R. MOKAYA. Hollow spheres of crystalline porous metal oxides: A generalized synthesis route via nanocasting with mesoporous carbon hollow shells. *Journal of Materials Chemistry* [online]. 2005, **15**(30), 3126–3131. ISSN 09599428. doi:10.1039/B502558C

[20] LI, S., A. PASC, V. FIERRO and A. CELZARD. Hollow carbon spheres, synthesis and applications – a review. *Journal of Materials Chemistry A* [online]. 2016, **4**(33), 12686–12713. ISSN 2050-7496. doi:10.1039/C6TA03802F

[21] KOLMAN, D. and K. VOLENÍK. Modeling of Oxidation During Plasma Spraying of Iron Particles. *Plasma Chemistry and Plasma Processing volume* [Online]. 2002, **22**(3). ISSN 572-8986

[22] VOLENÍK, K., J. LEITNER, E. HANOUSEK, J. DUBSKY and B. KOLMAN. Oxides in Plasma-Sprayed Chromium Steel. *Journal of Thermal Spray Technology* [Online]. 1997, **6**, 327-334. ISSN 2379-1551.

[23] MATĚJÍČEK, J., T. KAVKA, R. MUŠÁLEK, P. CTIBOR, J. MEDŘICKÝ, M. VILÉMOVÁ, B. NEVRLÁ, S. DEGOT and A. DENOIRJEAN. Tungsten-steel composites and FGMs prepared by argon-shrouded plasma spraying. *Surface and Coatings Technology* [online]. 2021, **406**, 126746. ISSN 0257-8972. doi:10.1016/J.SURFCOAT.2020.126746

[24] KAMBARA, M., M. FUKUDA, R. OHTA, T. TANAKA, A. TAKEUCHI, M. DOUGAKIUCHI and K. FUKUDA. Effect of powder loading on plasma spheroidization of hydride-dehydride titanium powders. *Japanese Journal of Applied Physics* [online]. 2021, **60**(10), 105507. ISSN 1347-4065. doi:10.35848/1347-4065/AC28E1

[25] KANAGARAJ, S., M. S.A. OLIVEIRA and J. A. DE OLIVEIRA SIMÕES. *Tribology of biocomposites* [online]. B.m.: Elsevier Inc., 2009. ISBN 9781845694364. doi:10.1533/9781845697372.3.441

[26] GANVIR, A., S. NAGAR, N. MARKOCSAN and K. BALANI. Deposition of hydroxyapatite coatings by axial plasma spraying: Influence of feedstock characteristics on coating microstructure, phase content and mechanical properties. *Journal of the European Ceramic Society* [online]. 2021, **41**, 4637–4649. doi:10.1016/j.jeurceramsoc.2021.02.050

[27] BAO, Y. *Plasma Spray Deposition of Polymer Coatings*. *Disertation thesis*. Uxbridge: Department of Materials Technology, Brunel University, 1995.

[28] BECKERS, D., N. ELLENDT, U. FRITSCHING and V. UHLENWINKEL. Impact of process flow conditions on particle morphology in metal powder production via gas atomization. *Advanced Powder Technology* [online]. 2020, **31**(1), 300–311. ISSN 0921-8831. doi:10.1016/J.APT.2019.10.022

[29] BRUCE SEE, J. and G. H. JOHNSTON. Interactions between nitrogen jets and liquid lead and tin streams. *Powder Technology* [online]. 1978, **21**(1), 119–133. ISSN 00325910. doi:10.1016/0032-5910(78)80115-6

[30] TOMASZEK, R., L. PAWLOWSKI, L. GENGEMBRE, J. LAUREYNS, Z. ZNAMIROWSKI and J. ZDANOWSKI. Microstructural characterization of plasma sprayed TiO2 functional coating with gradient of crystal grain size. *Surface and Coatings Technology* [online]. 2006, **201**(1–2), 45–56. ISSN 02578972. doi:10.1016/J.SURFCOAT.2005.10.033

[31] What are the industrial issues with powders? [online]. [accessed. 2022-07-02]. https://ametek.com/

[32] BOULOS, M. I. Thermal Plasma Processing. *IEEE Transactions On Plasma Science.* 1991, **19**(6), [online]. doi:10.1109/27.125032

[33] Standard Test Methods for Flow Rate of Metal Powders Using the Hall Flowmeter Funnel. ASTM B213 [online]. https://compass.astm.org/document/?contentCode=ASTM%7CB0213-20%7Cen-US

[34] Standard Test Method for Sieve Analysis of Metal Powders. ASTM B214 [online]. https://compass.astm.org/document/?contentCode=ASTM%7CB0214-16%7Cen-US

[35] YE, Z., X. JIANG and Z. WANG. Measurements of Particle Size Distribution Based on Mie Scattering Theory and Markov Chain Inversion Algorithm. *Journal of software* [online]. 2012, **7**(10). doi:10.4304/jsw.7.10.2309-2316

[36] BLACK, D. L., M. Q. MCQUAY and M. P. BONIN. Laser-based techniques for particle-size measurement: A review of sizing methods and their industrial applications. *Progress in Energy and Combustion Science* [online]. 1996, **22**(3), 267–306. ISSN 03601285. doi:10.1016/S0360-1285(96)00008-1

[37] VAN DER BILT, A., J. H. ABBINK, F. MOWLANA and M. R. HEATH. A comparison between data analysis methods concerning particle size distributions obtained by mastication in man. *Archives of Oral Biology* [online]. 1993, **38**(2), 163–167. ISSN 00039969. doi:10.1016/0003-9969(93)90202-W

[38] BAHAR BASIM, G. and M. KHALILI. Particle size analysis on wide size distribution powders; Effect of sampling and characterization technique. *Advanced Powder*

Technology [online]. 2015, **26**(1), 200–207. ISSN 15685527. doi:10.1016/J.APT.2014.09.009

[39] BOSCHETTO, A. and V. GIORDANO. Powder sampling and characterization by digital image analysis. *Measurement: Journal of the International Measurement Confederation* [online]. 2012, **45**(5), 1023–1038. ISSN 02632241. doi:10.1016/J.MEASUREMENT.2012.01.041

[40] LI, Y. and K. A. KHOR. Effect of plasma spraying conditions on the spheroidization of zircon and alumina mixtures. *Journal of Materials Processing Technology* [online]. 1999, **89–90**, 532–537. ISSN 09240136. doi:10.1016/S0924-0136(99)00133-8

[41] CAHN, R. W. and E. M. LIFSHITZ. *Concise encyclopedia of materials characterization*. Pergamon Press Ltd., Oxford, England, 1993. ISBN 0-08-040603-3

[42] ZEVIN, L. S. and G. KIMMEL. Quantitative X-Ray Diffractometry. *Quantitative X-Ray Diffractometry* [online]. 1995. doi:10.1007/978-1-4613-9535-5

[43] STRELI, C., P. WOBRAUSCHEK and P. KREGSAMER. X-ray Fluorescence Spectroscopy, Applications. *Encyclopedia of Spectroscopy and Spectrometry* [online]. 1999, 2478–2487. doi:10.1006/RWSP.2000.0337

[44] *Lectures by prof. Karlík and prof. Haušild.* DM-FNSPE-CTU, 2020-2022.

[45] CULLITY, B. D. *Elements of X-ray Diffraction* [online]. Prentice Hall, New Jersey, USA, 2001. ISBN 0-201-61091-4

[46] RIETVELD, H. M. and IUCR. A profile refinement method for nuclear and magnetic structures. *urn:issn:0021-8898* [online]. 1969, **2**(2), 65–71. ISSN 0021-8898. doi:10.1107/S0021889869006558

[47] YOUNG, R. The Rietveld Metod. *Climate Change 2013 - The Physical Science Basis* [online]. 1993, 293. ISSN 0232-1300.

[48] PAKSERESHT, A. H., M. R. RAHIMIPOUR, M. R. VAEZI and M. SALEHI. Thermal plasma spheroidization and spray deposition of barium titanate powder and characterization of the plasma sprayable powder. *Materials Chemistry and Physics* [online]. 2016, **173**, 395–403. ISSN 02540584. doi:10.1016/J.MATCHEMPHYS.2016.02.028

[49] BOATEMAA, L., J. C. BROUWER, S. VAN DER ZWAAG and W. G. SLOOF. The effect of the TiC particle size on the preferred oxidation temperature for self-healing of oxide ceramic matrix materials. *Journal of Materials Science* [online]. 2018, **53**(8), 5973–5986. ISSN 15734803. doi:10.1007/S10853-017-1973-X

[50] *abcr Gute Chemie* [online]. [accessed. 2022-07-02]. https://abcr.com/de_en/ab425674

[51] KIRBY, R. K. Thermal Expansion of Rutile from 100 to 700 °K *. *Physics and Chemistry*. 1967, **71**(5).